AD-A091 558 HUGHES RESEARCH LABS MALIBU CA F/G 20/6
LOW-LOSS FIBER WAVEGUIDES.(U)
OCT 80 J A HARRINGTON N00014-79-C-0691
UNCLASSIFIED NL

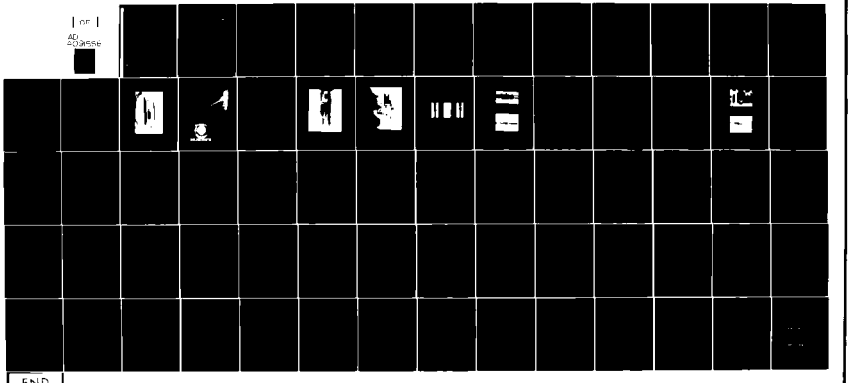

END
DATE FILMED
12-80
DTIC

LEVEL II

LOW-LOSS FIBER WAVEGUIDES

James A. Harrington

Hughes Research Laboratories
3011 Malibu Canyon Road
Malibu, CA 90265

October 1980

N00014-79-C-0691

Annual Technical Report
For period 1 August 1979 through 31 July 1980

Approved for public release; distribution unlimited.

Sponsored by

MATERIAL SCIENCES DIVISION
OFFICE OF NAVAL RESEARCH
800 North Quincy Street
Arlington, Virginia 22217

UNCLASSIFIED

SECURITY CLASSIFICATION OF THIS PAGE (When Data Entered)

REPORT DOCUMENTATION PAGE	READ INSTRUCTIONS BEFORE COMPLETING FORM
1. REPORT NUMBER	2. GOVT ACCESSION NO. AD-A091558	3. RECIPIENT'S CATALOG NUMBER
4. TITLE (and Subtitle) LOW-LOSS FIBER WAVEGUIDES.	5. TYPE OF REPORT & PERIOD COVERED Annual Technical Report, 1 Aug 1979 — 31 Jul 1980
	6. PERFORMING ORG. REPORT NUMBER
7. AUTHOR(s) James A. Harrington	8. CONTRACT OR GRANT NUMBER(s) N00014-79-C-0691
9. PERFORMING ORGANIZATION NAME AND ADDRESS Hughes Research Laboratories 3011 Malibu Canyon Road Malibu, California 90265	10. PROGRAM ELEMENT, PROJECT, TASK AREA & WORK UNIT NUMBERS
11. CONTROLLING OFFICE NAME AND ADDRESS Material Sciences Division Office of Naval Research 800 North Quincy St., Arlington, VA 22217	12. REPORT DATE Oct 1980
	13. NUMBER OF PAGES
14. MONITORING AGENCY NAME & ADDRESS (if different from Controlling Office)	15. SECURITY CLASS. (of this report) UNCLASSIFIED
	15a. DECLASSIFICATION DOWNGRADING SCHEDULE

16. DISTRIBUTION STATEMENT (of this Report)

Approved for public release; distribution unlimited.

17. DISTRIBUTION STATEMENT (of the abstract entered in Block 20, if different from Report)

18. SUPPLEMENTARY NOTES

19. KEY WORDS (Continue on reverse side if necessary and identify by block number)

Infrared fibers, optical materials, fiber optics, light scattering.

20. ABSTRACT (Continue on reverse side if necessary and identify by block number)

This annual report summarizes our efforts to fabricate low-loss fiber waveguides with potential loss near ~~10/3~~ dB/km. To develop such low-loss fibers requires producing fiber from unconventional, non-oxide materials such as the metal halides or some special fluoride glasses. Specifically, our approach has been to use alkali and thallium halides

DD FORM 1 JAN 73 1473 EDITION OF 1 NOV 65 IS OBSOLETE

UNCLASSIFIED

SECURITY CLASSIFICATION OF THIS PAGE (When Data Entered)

17260

because these crystalline materials have, in the case of KCl, some of the lowest bulk losses measured to date at IR wavelengths.

The first method we used to fabricate KCl fiber was extrusion. Although this method had worked well for the thallium halides, it proved unsuccessful for KCl and other alkali halides. In every case, we found that extruded KCl (or CsI and $PbCl_2$) fiber had an irregular, fish-scale surface, from which we concluded that extrusion techniques should be abandoned for the alkali halides.

Based on these results, we began to develop new fiber-fabrication methods for KCl. The method chosen for study was hot rolling. The advantage of hot rolling over extrusion is that there is less friction between the fiber and forming surface (roller or die) and smaller reductions per pass. At this point, we have made one 50-cm-long KCl fiber with improved surface quality (compared to extrusion). Further work on hot rolling is planned next year.

Studies of the optical properties of our fibers and bulk materials concentrated on determining the scattering and absorption contributions to the total attenuation. For the first time, we measured the scattering loss in fibers at 10.6 μm using an integrating sphere. Our measurements showed that, for KRS-5 (TlBrI) fibers, the absorptive and scattering losses were approximately equal. Similar results were obtained in bulk KCl single crystals from our Rayleigh-Brillouin light-scattering measurements. These significant results indicate that better fibers should result from the use of higher-purity starting material and improved fabrication techniques. During the next year, we will use purified thallium halides and explore other fiber-forming methods, such as single-crystal fiber growth, to fabricate lower-loss fiber.

TABLE OF CONTENTS

SECTION		PAGE
	PREFACE	7
1	INTRODUCTION AND SUMMARY	9
2	TECHNICAL PROGRESS AND DISCUSSION	13
	A. General Considerations	13
	B. Fiber Materials	15
	C. Fiber Fabrication	16
	D. Optical Evaluation	28
3	FUTURE PLANS AND RECOMMENDATIONS	43
	REFERENCES	45
APPENDIX:	SCATTERING LOSSES IN SINGLE AND POLYCRYSTALLINE MATERIALS FOR INFRARED FIBER APPLICATIONS	47

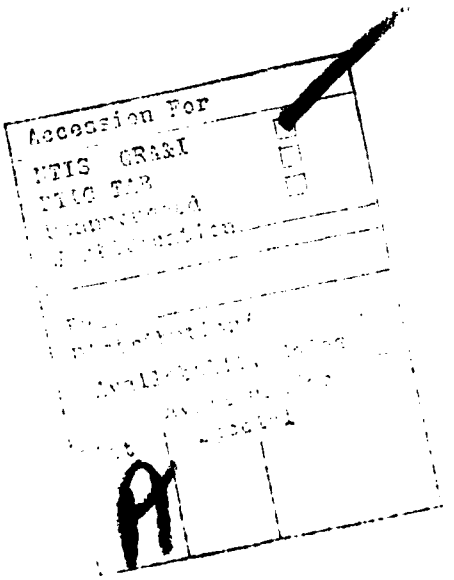

LIST OF ILLUSTRATIONS

FIGURE		PAGE
1	Large extruder for making billets or fiber	17
2	Extruded polycrystalline rod for use as starting billet in small fiber extruder	18
3	Heel of KRS-5 billet showing 4:1 area reduction used to make billets	18
4	Overall view of extruder showing controls and fiber take-up reel	20
5	Detail of extruder controls showing temperature and pressure controls and extrusion chamber	21
6	Extruded KCl fiber showing irregular surface structure	22
7	Extruded lead chloride fiber	23
8	Schematic of hot rollers	25
9	KCl stuck in roller groove after only three reductions	27
10	Etched surface of rolled KCl fiber	27
11	CO_2 laser insertion loss apparatus	29
12	Scattering sphere measurements on KRS-5 fiber at 10.6 μm	33
13	Integrated scattering data obtained from data in Figure 12	37

PREFACE

This interim technical report describes development work on low-loss fiber waveguides performed during the period 1 August 1979 to 31 July 1980. This period represents the first year of work on this research program.

The principal investigator was James A. Harrington. Assisting in the program were Arlie Standlee, who extruded the fibers and made many of the optical measurements; Roger Turk and Nelson Ramirez, who developed the hot rolling techniques for fiber fabrication; and Bradley Bobbs and Rubin Braunstein, who performed the Rayleigh-Brillouin light-scattering studies.

SECTION 1

INTRODUCTION AND SUMMARY

For the past four years, Hughes Research Laboratories (HRL) has been actively engaged in the development of highly transmitting infrared (IR) fiber waveguides for use in sensor and communication systems and for applications requiring power delivery, such as in CO_2 laser surgery. During this time, IR fibers fabricated from KRS-5 (thallium bromoiodide) have successfully been used in short lengths (less than 2 m) to relay information to cooled-focal-plane arrays; to receive coded CO_2-TEA laser pulses and transmit this information to photodetectors; and to deliver up to 9 W of cw, CO_2 laser radiation for heating and cutting. Future systems needs will require longer lengths of high-transparency fiber. In particular, long-distance communication links may take advantage of the extremely low loss potential ($\sim 10^{-3}$ dB/km) predicted theoretically for a large class of IR fiber materials near 5 μm. To realize this potential, however, the optical properties of our fibers must be significantly improved over the current lowest loss of 300 dB/km (KRS-5 fiber).

The primary objective of the present research program is the development of low-loss fiber waveguides whose potential loss is near 10^{-3} dB/km. Our approach to developing these waveguides has been the extrusion of polycrystalline thallium and alkali halide fibers. The alkali halides were chosen for their high purity and especially high transparency (measured in bulk single crystals). KCl, for example, has a measured bulk loss of 0.4 dB/km at 5.2 μm. Although the alkali halides have lower loss than do the thallium or silver halides, they are far less ductile and, therefore, have not readily been adapted to the extrusion process. The thallium halides have yielded the best optical IR fibers to date. For KRS-5 and TlBr, measured bulk and fiber losses are essentially equal at 10.6 μm, and further improvement (two orders of magnitude are theoretically possible at 10.6 μm and much more at 5 μm) will require purer starting material.

Our development of low-loss waveguides has, during this first year of ONR-supported research, emphasized three related areas of research:

- Fiber billet preparation
- Fiber fabrication
- Optical evaluation and analysis.

We began the year by carefully selecting the low-loss starting materials that we felt had the greatest potential for fabrication into highly transparent fibers. The materials we chose were reactive atmosphere processed (RAP) alkali halides and thallium halides. The alkali halides, and KCl in particular, are materials that had proven to be some of the lowest-loss crystalline materials ever measured at IR wavelengths. These materials, however, had not successfully been fabricated into fibers. The thallium halides are an ideal choice because they are more ductile than the alkali halides and they have been successfully extruded into the best transmitting IR fibers made to date. Their losses, however, are not as low as bulk KCl.

The results of our extrusion experiments on KCl were quite discouraging. We found that, using many different extrusion parameters (such as temperature, pressure, quench-gas flow, ambient atmosphere, type of lubricant), we were unable to produce good-quality KCl fiber by extrusion. In general, the surface quality was poor, exhibiting a fish-scale appearance that resulted from friction between the die and the surface of the fiber. We have to conclude that extrusion, although successful for the ductile thallium halides, is not a good method for the alkali halides.

Based on these results, we decided to abandon the extrusion process for all materials except the thallium halides. As an alternative fiber fabrication technique for the alkali halides, we began developing a hot-rolling method. In this method, the billet is successively reduced, in small reductions per pass, to a polycrystalline fiber. The advantage of rolling over extrusion is reduced friction between the roller and billet material (rolling versus sliding friction) and smaller reductions. At this point in the program, we have demonstrated hot rolling of KCl. The

first fiber produced, although rather lossy, did not have the fish-scale surface produced in extrusion. We are encouraged by these results, and further work with better-quality rollers will be carried out during the second year of the program.

The cornerstone of our fiber development is the evaluation and analysis of fiber and bulk materials. In the past, we have routinely measured the insertion loss, α_T, of our fibers at 10.6 μm. This year for the first time we have also measured the scattering losses, α_S, directly in both fiber and bulk materials. Since α_T is the sum of α_S and the absorptive losses, α_A, we are now able to get a better understanding of the individual mechanisms contributing to the total fiber losses. For our extruded, polycrystalline KRS-5 fibers, we found, by using an integrating sphere in our measurements, that α_S and α_A are approximately equal. This significant result tells us that better fiber should result both from using higher purity starting material and improved fabrication techniques. In the next year of the program, we will be using RAP Tl-halides to, we hope, reduce scattering and absorptive losses; we also will be exploring other methods, such as single-crystal fiber growth, to minimize α_S.

After one year of development effort on low-loss fibers, we have reached the following conclusions:

- The extrusion of alkali halides is not feasible
- The new technique of hot rolling, developed in part under this contract, appears promising for fabricating alkali halide fibers
- Extruded KRS-5 fibers continue to be the best IR fibers although their present losses (0.4 dB/m at 10.6 μm) are many orders of magnitude above the theoretical limit
- Scattering and absorptive losses are, as shown for the first time on this program, approximately equal in KRS-5 fiber. This suggests that both the purity of the material and the fiber fabrication technique are important if fibers are to be made with the projected losses of 10^{-3} dB/km.

Based on these conclusions, we make the following recommendations for next year's efforts:

- Develop further hot rolling of alkali halide fibers
- Study single-crystal (SC) fiber growth of alkali halides. We feel that SC fibers should be the ultimate fiber because of the small residual scattering expected.
- Continue study of individual loss mechanisms in fiber and bulk materials. These studies will again be used to provide feedback to both our material purification work and our fiber fabrication technology so that a better fiber can be produced.
- Launch a small study aimed at cladding our waveguides. Both pre- and post-fabrication cladding techniques will be investigated.

SECTION 2

TECHNICAL PROGRESS AND DISCUSSION

A. GENERAL CONSIDERATIONS

To develop fiber waveguides with losses well below those of conventional silica waveguides (0.25 dB/km at 1.6 μm)[1] requires using a new class of materials and novel fiber fabrication techniques. The materials that show the greatest promise for ultralow loss fall into two categories: nonoxide glasses and crystalline solids. In the first category, the noncrystalline materials of interest include BeF_2,[2] mixed fluoride glasses,[3,4] and $ZnCl_2$.[2] Several investigators have successfully grown large pieces of multicomponent fluoride glasses (such as ZrF_4-ThF_4-BaF_2)[3] and, in some cases, have drawn fibers from these glasses (lowest fiber loss reported[5] is 0.45 dB/m at 3.39 μm). In addition to materials purity, many problems still remain to be solved before nonoxide glasses can be fabricated into highly transparent waveguides. (One serious problem, for example, is devitrification of the glass in either bulk or fiber form). Our approach to developing extremely low loss fibers is to concentrate our efforts in the second category, crystalline solids.[6-9] Although crystalline materials such as the alkali and thallium halides are unfortunately not amenable to fiber formation using conventional fiber-drawing techniques, they nevertheless have exhibited some of the lowest losses measured[10] (KCl loss was 10^{-6} cm^{-1}, or 0.4 dB/km at 4.2 μm). The approaches that we have tried in fabricating fiber from halide crystals include extrusion, hot rolling, and single crystal fiber growth. Our best polycrystalline (extruded) fiber has been KRS-5 (TlBrI) with losses of 0.4 dB/m at 10.6 μm.

The successful development of new fibers for future long-distance communications links will involve a combined research effort in three interrelated areas: materials preparation, fiber fabrication, and evaluation. During this first year of the program, we have addressed each area, but paid greatest attention to evaluation and analysis. In particular, making a better waveguide than the present KRS-5 fiber will require purer starting material and a suitable fiber forming technology.

Our extensive past work on the Tl halides (notably KRS-5) has enabled us to extrude our best polycrystalline fiber even though this fiber is well above the theoretical limit ($<10^{-3}$ dB/km at 6 μm) for this material. KRS-5, moreover, is ductile and therefore readily lends itself to the hot extrusion process for fiber formation. The alkali halides, however, have much lower bulk losses than the thallium halides. This is a result of the many years of development on these materials for applications as high-energy laser windows. During the past decade, reactive atmosphere processing[11] has been developed for the alkali halides, with the result that extremely high-purity, low-loss KCl, KBr, and NaCl are available for fiber research. Unfortunately, our extensive research on extruding KCl has shown that this material and probably the alkali halides in general cannot be extruded into good-quality fiber. The best extruded KCl fiber (500 μm diameter, 25 cm long) had a loss of 4.2 dB/m at 10.6 μm; this is 10 times greater than the loss for KRS-5 and orders of magnitude greater than KCl's projected intrinsic loss (see Appendix). We found that the losses in KCl fiber resulted from the poor surface quality of the fiber (surface had fish-scale appearance). The surface irregularities are caused in the extrusion process by friction between the diamond die and the KCl. We concluded from our work that this friction cannot be reduced sufficiently for any alkali halide to be extruded successfully and hence that alternative fiber fabrication techniques must be used. Two methods that show promise for the alkali halides (KCl in particular) are hot rolling and single-crystal fiber growth. Section 2.C describes our efforts to hot roll KCl into optical fiber.

A thorough analysis of our bulk materials and fibers is essential for understanding the fundamental loss mechanisms. Our basic loss measurements include fiber insertion loss at 10.6 and 5.2 μm, RB scattering on bulk KCl, and scattering studies on KRS-5 fiber at 10.6 μm using an integrating sphere. These measurements have helped us correlate the optical and structural properties of our polycrystalline waveguides (for example, fiber grain size as a function of transmission) as well as learn about the fraction (of the total fiber attenuation) that is scattered out of the fiber. In one instance, we determined that the

output end of our fiber scattered light excessively and that this loss could be significantly reduced by using a different end-polishing technique.

B. FIBER MATERIALS

In principle, there are many crystalline materials with the potential for extremely low loss. But in practice, the choice of material is severely limited by the available fabrication techniques. The extrusion process, for example, requires a ductile material. Those materials which have already proven suitable for extrusion include the thallium and silver halides. Table 1 lists these and other candidate materials and their melting points. In general, the lower melting point solids are malleable and lend themselves to the extrusion process. In this process, the area reductions are greater than 100:1 (typically 450:1). For the Tl and Ag halides, this reduction does not lead to a fish scaled surface as it does in the alkali halides. Instead, the fiber surface is smooth because the surfaces of these ductile materials are reconstituted on passing through the diamond extrusion die.

In an effort to find new materials (other than the Tl and Ag halides) that are extrudable into fiber, we prepared billets from several of the other materials in Table 1. Specifically, we made billets from our own $PbCl_2$ and from Harshaw NaF and LiF. Lead chloride was chosen, even though it is not cubic (orthorhombic), because its melting point falls midway between that of the Tl (extrudable) and K (not extrudable) halides. Sodium and lithium fluoride were selected for limited study only because we had not tried a fluoride compound and felt that the extrusion properties of fluorides might differ from those of the other alkali halides. The billets prepared were 5.3 mm in diameter by approximately 7.5 cm in length.

In addition to these "new" materials, KCl and KRS-5 were also prepared in billet form. We selected RAP-grown KCl prepared earlier in our laser window research programs. Billets of this high-purity, low-absorption (2 to 4 x 10^{-4} cm^{-1} at 10.6 μm) material were used in our hot rolling experiments. We used single-crystal billets of KRS-5

Table 1. Melting Point of Some Fiber Materials

Material	Melting Point, °C
Thallium bromoiodide (KRS-5)	414.5
Silver chloride (AgCl)	457.7
Thallium bromide (TlBr)	460
Lead chloride ($PbCl_2$)	501
Potassium chloride (CKl)	776
Lithium fluoride (LiF)	870
Sodium fluoride (NaF)	992
Cadmium telluride (CdTe)	1000
Gallium arsenide (GaAs)	1238
Zinc selenide (ZnSe)	1525

purchased from Harshaw Chemical Co. Since we wished to use polycrystalline material for some experiments, we converted several 12-mm-diameter Harshaw billets into long, polycrystalline rods for use as starting billets on our small fiber extruder. The conversion was done by placing the original billets into a large extrusion press (shown in Figure 1) and extruding them. One of these rods (∿38 cm long) is shown in Figure 2. The heel of the extruded KRS-5 billet is shown in Figure 3 (this shows the 4:1 reduction used). The long rods were cut into 7.5-cm-long pieces for extrusion into fiber.

C. FIBER FABRICATION

1. Extrusion

The hot extrusion of crystalline materials into fibers continues to be our best method of fiber fabrication.[6-8] This method has proven highly successful for the ductile thallium[6-8] and silver halides,[9] but unsuccessful for alkali halides such as KCl. During this past year, we extruded KCl, $PbCl_2$, and KRS-5 into optical fiber using our small extruder (uses 5.3-mm-diameter starting billets). This extruder,

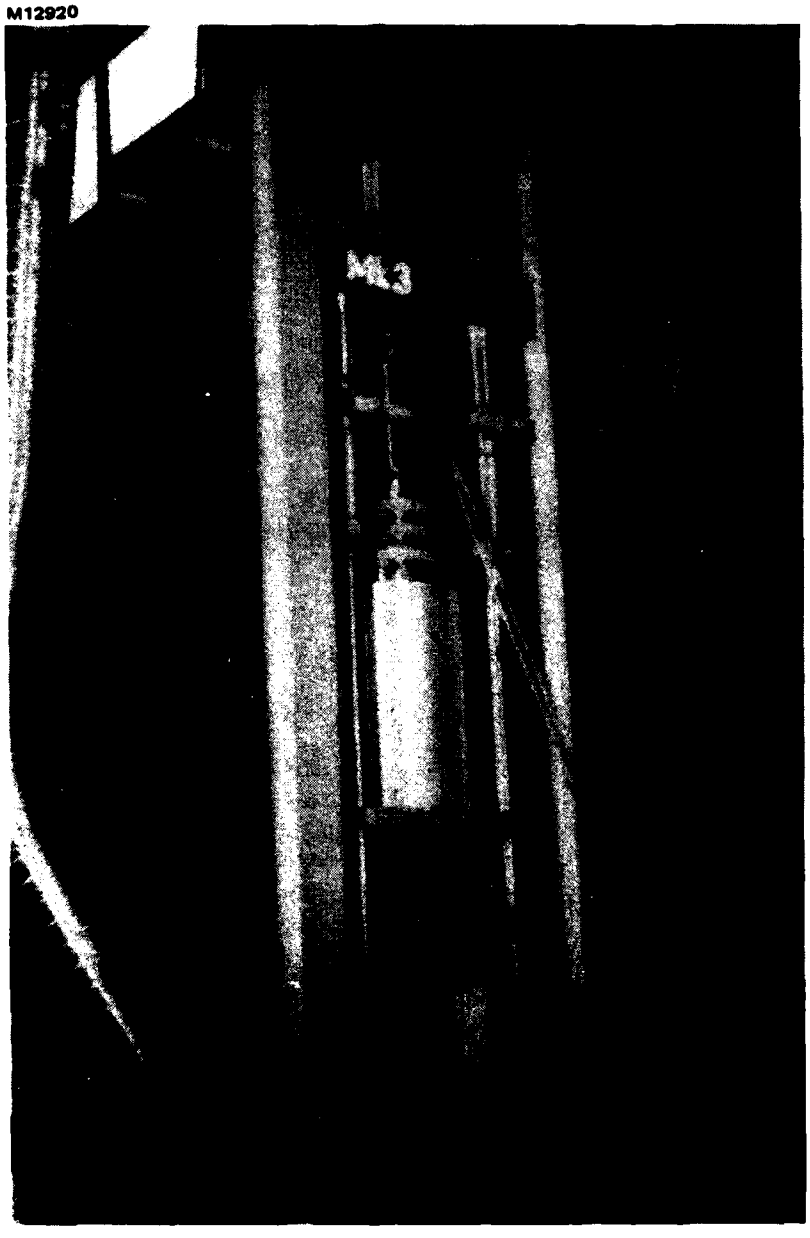

Figure 1. Large extruder for making billets or fiber.

M13299

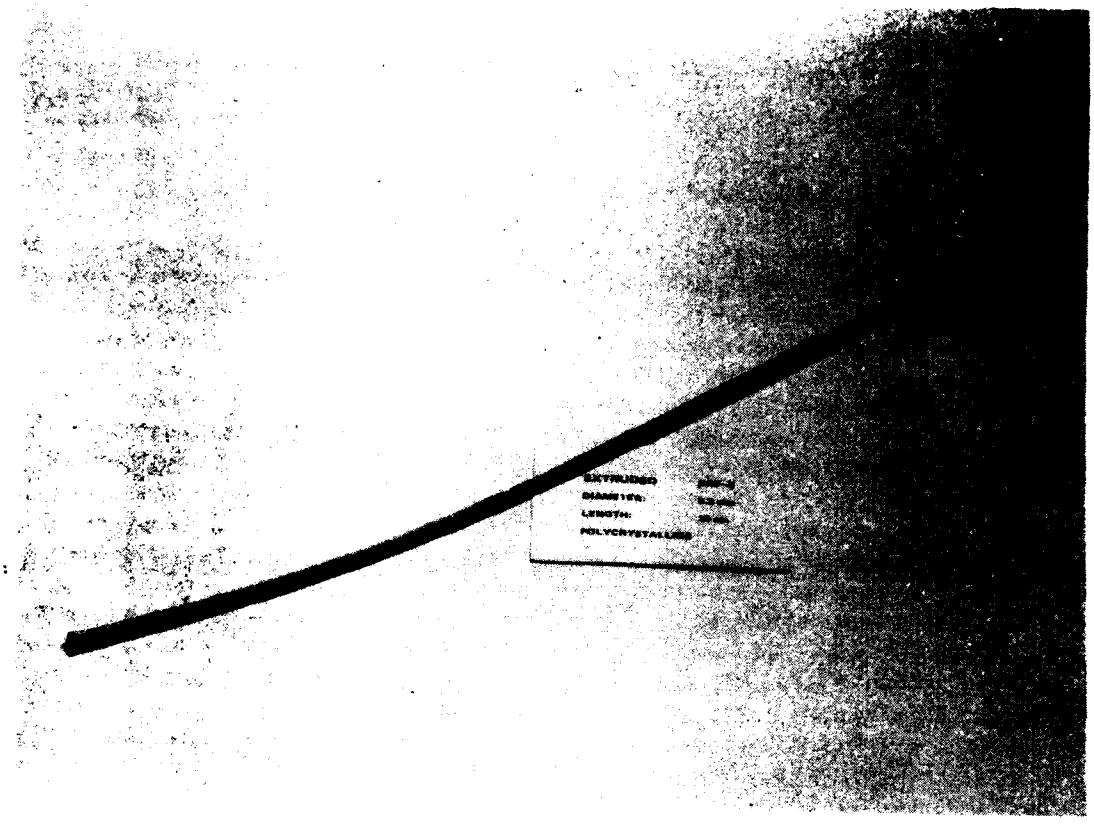

Figure 2. Extruded polycrystalline rod for use as starting billet in small fiber extruder.

9888-1

Figure 3. Heel of KRS-5 billet showing 4:1 area reduction used to make billets.

shown in Figures 4 and 5, can automatically spool the fiber (sometimes used for KRS-5), but most experimental fiber is removed in 1-m lengths for measurement. Temperatures up to 800°C are possible.

To take advantage of our high-quality (RAP) KCl, we launched an extensive research program, funded in part by RADC, to extrude KCl fiber. After two years' research, we are forced to conclude that it is not possible to extrude low-loss KCl fiber. From these results as well as limited results for CsI, we feel that it is unlikely that, as a class, the alkali halides are extrudable.

A variety of experimental conditions were used in the KCl extrusion. In summary (further details may be found in the Final Technical Report, Contract No. F19628-78-C-D109, September 1980 sponsored by RADC), we tried lubricants, inert atmospheres, temperatures between 25 and 740°C, different die materials (tungsten carbide and diamond), and reduction ratios from 400:1 to 4:1 all without success. In general, the KCl fiber surface was irregular (often fish scaled), and the fiber had the poor optical properties expected from such poor surfaces. Figure 6 (taken from the RADC report) illustrates the problems we encountered in extruding KCl. Even at high temperatures (740°C), the surface of the fiber was poor. These results have led us to abandon attempts to extrude KCl in favor of the more promising fabrication techniques of hot rolling and single-crystal fiber growth.

We made a limited effort to extrude $PbCl_2$. Although not cubic, we felt $PbCl_2$ to be worth study because it is more ductile than the alkali halides. With a melting point of 501°C, it falls between the melting points of the Tl and Ag halides and the alkali halides (see Table 1). Therefore, we felt that $PbCl_2$ may be more extrudable than KCl.

The extrusion of 500-μm-diameter $PbCl_2$ fiber was carried out at temperatures between 250 and 425°C using slow (1 mm/hr) and fast (1 cm/min) extrusion rates. In every case, the fiber was brittle and the surface appeared cloudy. Photomicrographs (Figure 7) revealed a fish-scaled surface similar to that obtained for KCl. Evidently, $PbCl_2$ does not behave like the Tl and Ag halides and we conclude that this is not a good material to extrude into optical fibers.

M13616

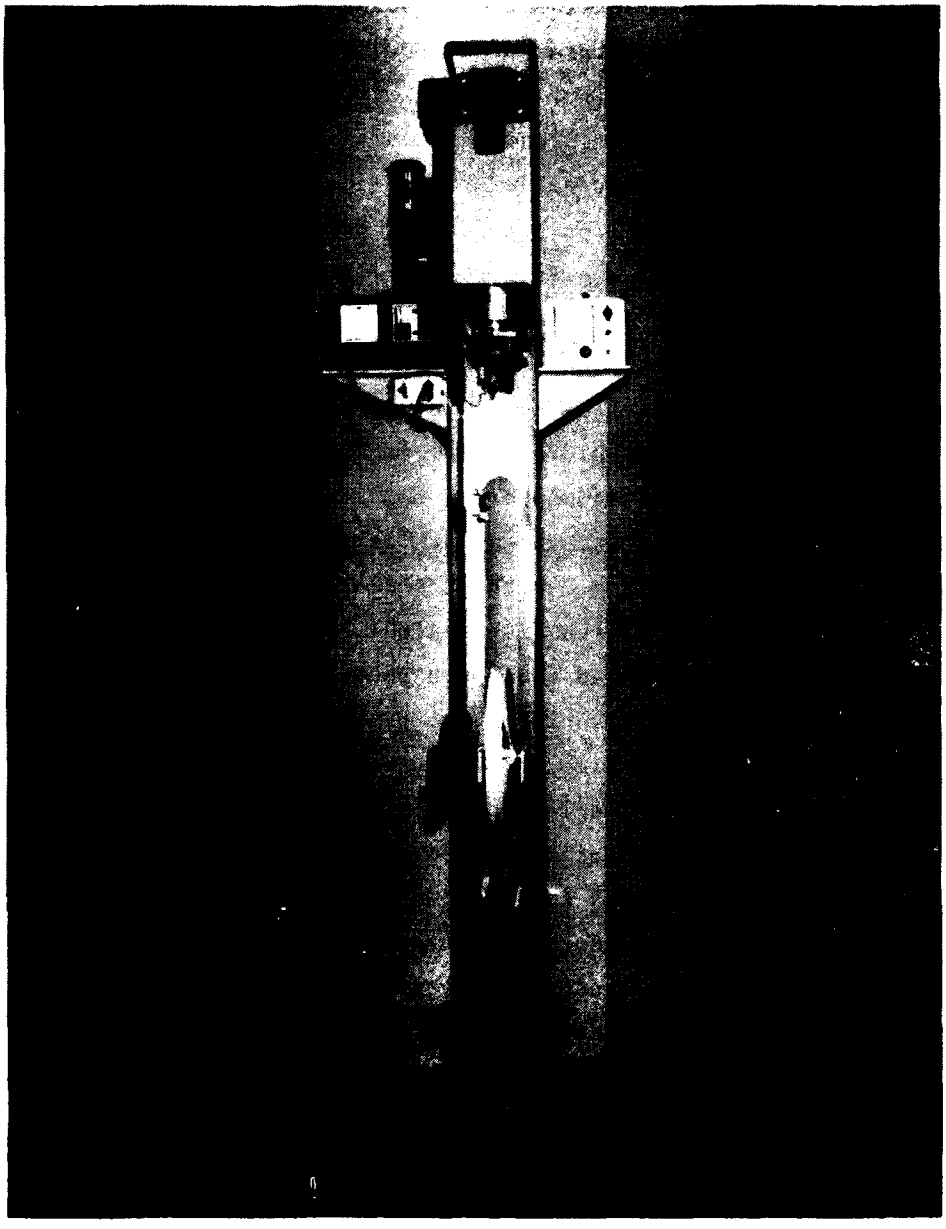

Figure 4. Overall view of extruder showing controls and fiber take-up reel.

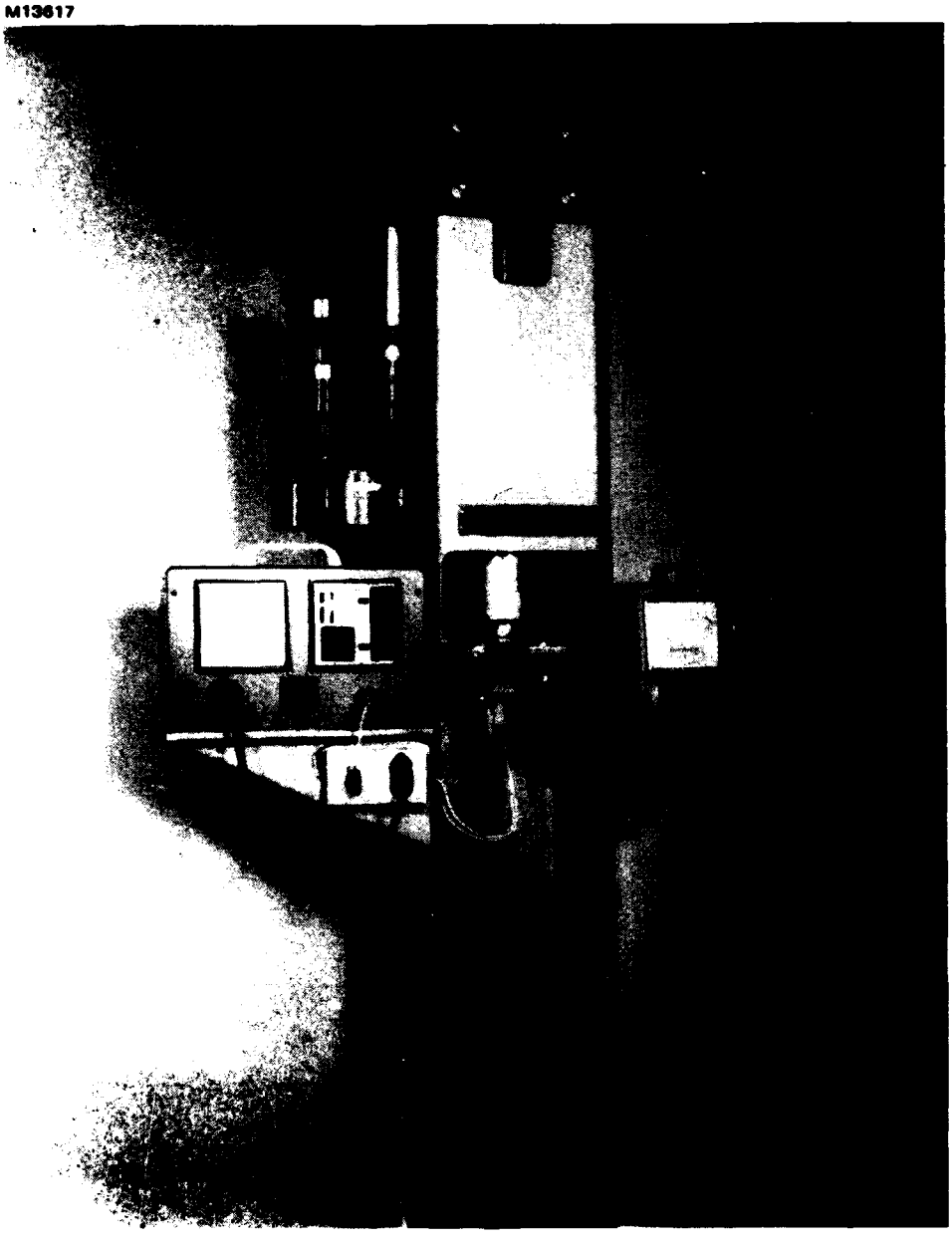

Figure 5. Detail of extruder controls showing temperature and pressure controls and extrusion chamber.

9508-4

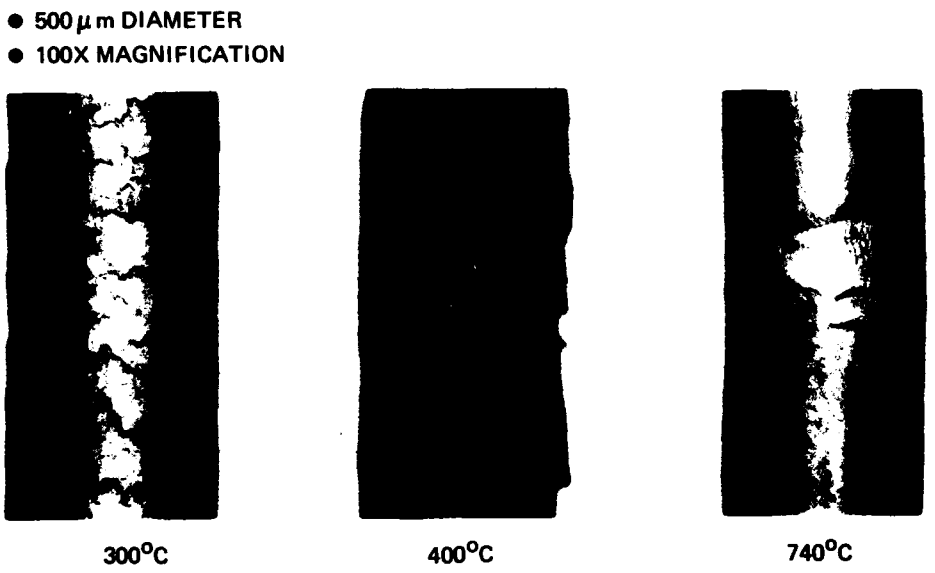

Figure 6. Extruded KCl fiber showing irregular surface structure.

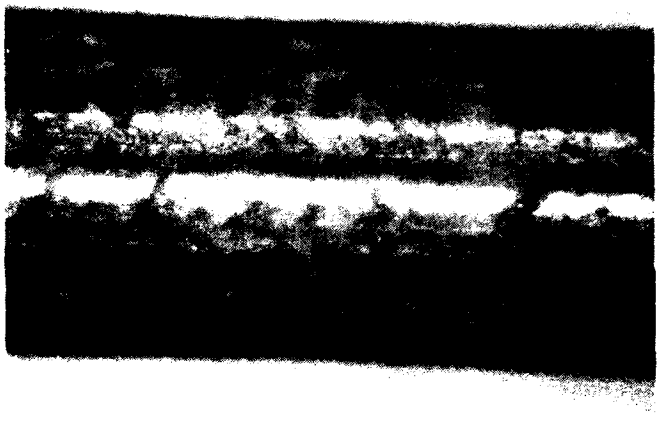

(a)

(b)

Figure 7. Extruded lead chloride fiber. Note fish-scale surface characteristic of the alkali halides. (a) 100x, (b) 200x.

Several KRS-5 fiber extrusion runs were made during the year to provide fiber for our optical and mechanical testing. Bare KRS-5 fiber (250 and 500 μm in diameter) was extruded. In a typical extrusion, 25 m of 25-μm-diameter and about 6 m of 500-μm-diameter fiber were obtained. Generally, the fiber was removed from the extruder in 1-m lengths and evaluated immediately (10.6-μm insertion loss measurement).

2. Hot Rolling

Hot rolling appears to be a promising technique for forming fibers from crystalline materials. We feel that it has several distinct advantages over extrusion, especially for the less ductile alkali halides. In the rolling process, there is less surface friction between the fiber and roll than is present between the fiber and die in extrusion. Furthermore, the area reduction per pass in rolling is considerably less than in extrusion. In our rollers, for example, the average reduction per pass is about 15%. In passing through the rollers, the fiber's surface is configured by the roller's surface. Since we can get a good optical finish on the rollers, the surface of the rolled fiber should also be of good optical quality. In general, hot rolling materials into fibers is a more gentle process than extrusion and, we hope, will produce fibers from KCl (and other materials) with smooth surfaces.

The hot-rolling apparatus used in this program was built around a commercial jewelry rolling mill. The rolling mill was modified for our application by adding heating elements (for temperatures up to 400°C) and a motor drive. The entire apparatus (see Figure 8) was enclosed in a sealed, insulated box so that an inert atmosphere (argon) could surround the rollers and sample during heating and rolling. The rollers themselves were polished and Ni plated to minimize sticking and to provide a good optical surface.

Our first series of experiments on rolling KCl (at 300°C) revealed that the KCl adhered to the roller grooves. Adhesion is a function of the finish on the roller and the shape of the groove. In this case, the grooves are round with ears at the point of contact between the upper and lower rollers. The purpose of the ears, which comprise 6.4% of the

9728–2

- HOT ROLLING

  ADVANTAGES

  - REDUCED FRICTION
  - SMALLER REDUCTION/PASS

  MATERIALS

  - KCl, KRS-5

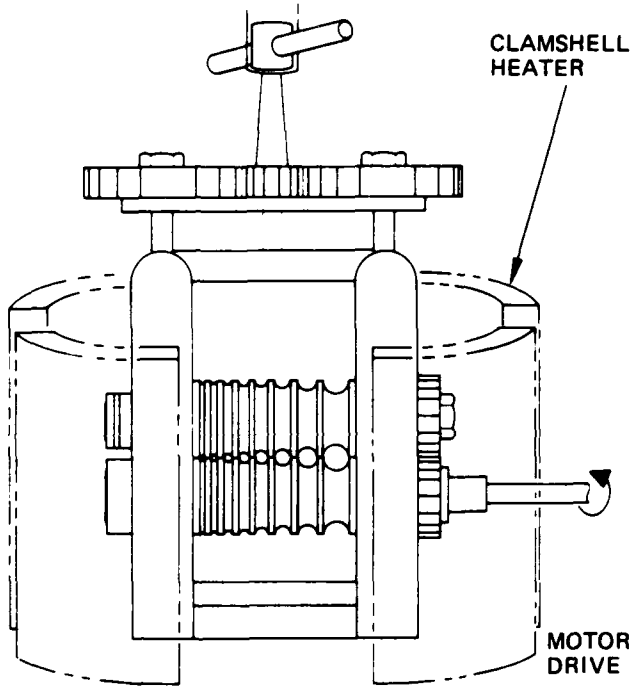

Figure 8. Schematic of hot rollers.

round groove area, is to allow for the expansion of the reduced material and hence to prevent flashing (material squeezed out between the rollers). But we found that KCl would overfill the ears and produce flashing unless the amount of reduction was carefully controlled. This flashing would in turn lead to adhesion between the KCl and the rollers. Figure 9 shows a piece of KCl stuck in a large groove as a result of the KCl overfilling the groove. In other cases, microscopic pits in the grooves created points for adhesion between the KCl and the metal. We were able to solve this problem by plating the rollers with copper followed by nickel to fill in the pits. Finally, the rollers were polished to an optical finish.

We had one successful hot rolling run on KCl. Beginning with a 0.200-in.-diameter single-crystal KCl rod, we successfully rolled a 0.060-in.-diameter (1.5-mm-diameter), 50-cm-long fiber. The rolling temperature was 300°C, and the linear velocity of rolling was 1.5 cm/min. The fiber was passed through 15 grooves, with an average reduction of 13.4% per groove. The rolled fiber surface was free of any fish scale. The photomicrograph given in Figure 10 shows the rolled KCl surface after etching in concentrated HCl. The average grain size appears to be about 25 μm for this fiber. Finally, the insertion loss measurement at 10.6 μm indicated a high loss of 23.7 dB/m for this fiber.

Although our initial studies show that hot rolling may be feasible for fabricating fibers, there remains considerable developmental work to be done before good-quality halide fibers can be produced. To improve our hot-rolling technique, we are procuring a new set of rollers with elliptical grooves and a finer optical finish. The final roller plating and polishing should help produce a better-surface-quality fiber (fiber surface takes on the roller finish), while the elliptical groove design should permit the fiber to expand more without flashing. In addition, the new rollers will have 28 grooves, with the smallest being 250 μm in diameter (the present rollers have 21 grooves, with the smallest being 500 μm in diameter).

Figure 9. KCl stuck in roller groove after only three reductions. Magnification is 4x.

Figure 10. Etched surface of rolled KCl fiber. Magnification 200x.

D. OPTICAL EVALUATION

The optical evaluation of both fiber and bulk materials provides the foundation of our understanding of loss mechanisms in transparent solids. Our loss measurements on fibers include independent measurements of the total attenuation coefficient (α_T) and the attenuation due to scattering (α_S).. The losses due to absorptive processes (α_A) are then calculated from the simple relationship

$$\alpha_T = \alpha_S + \alpha_A \quad .$$

From these measurements, we are able to relate the optical properties of our waveguides to the fiber's structural features, the fabrication process, and the material's purity.

The total attenuation coefficient α_T is determined by an insertion-loss measurement. Our CO_2 insertion-loss apparatus, shown in Figure 11, is conventional except for the addition of a ZnSe beam splitter used to monitor the incident power, I_o. The beam splitter is essential because the input end of the fiber reflects enough light (17%) to disturb the CO_2 laser cavity and thus change I_o. In this arrangement, the true I_o may be determined by noting the value of I_o at the time the transmitted intensity I_o is measured. This ensures that a reliable value of α_T is calculated.

During the first year of this program, numerous fiber loss measurements were made at 10.6 μm. In general, we found that the extruded KRS-5 fiber (250 and 500 μm diameter) had insertion losses that varied from 0.5 to 2.5 dB/m. The wide variation resulted from the use of different extrusion parameters (mainly extrusion temperature, speed, and quench gas temperature) and starting KRS-5 material (Harshaw Chemical Co. or British Drug House). Although we are not able to account, in detail, for the nature and source of the fiber loss, we have learned that certain extrusion parameters and the purity of the starting material are important if high quality fiber is to be fabricated. We have found, for example, that KRS-5 from Harshaw produces higher-quality fiber than KRS-5 from BDH. In fact, we found that not only was the initial

9508-8

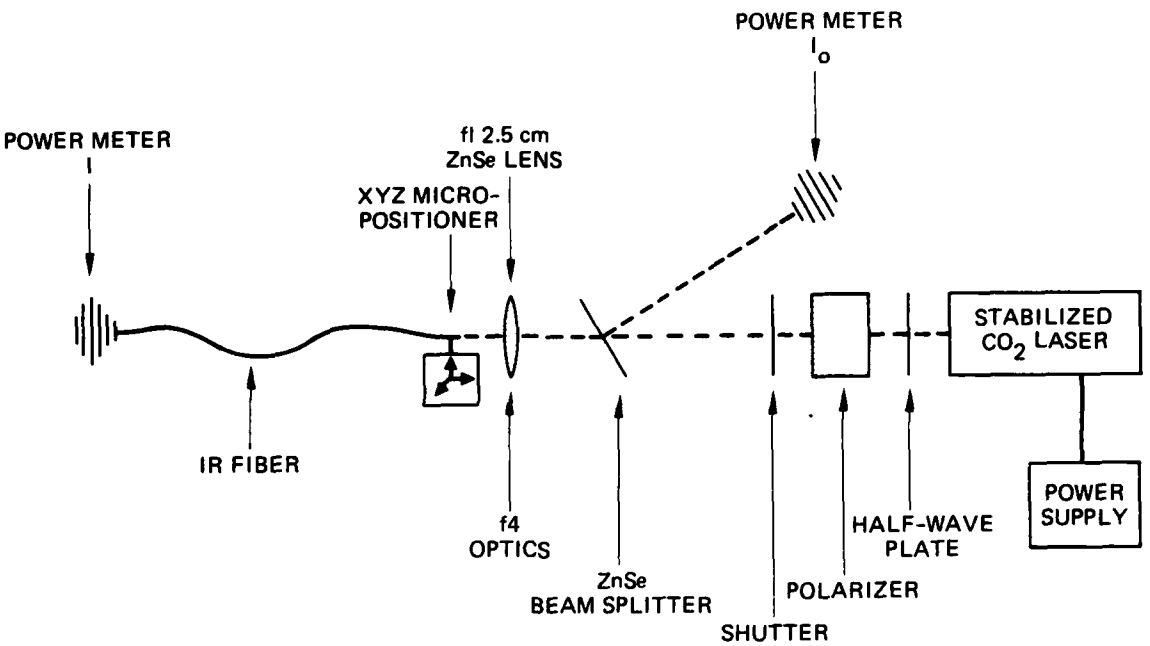

Figure 11. CO_2 laser insertion loss apparatus.

transmission of the BDH fiber worse, but also that its transmission degraded rapidly with time. In several cases, 1-m lengths of 500-μm-diameter BDH fiber had transmission coefficients of 45 to 55% (2.0 to 1.1 dB/m) immediately after extrusion which declined to less than 5% (11.6 dB/m) within 48 hr. This effect, which we have only seen in BDH material, is most likely due to impure starting material. We feel that their KRS-5 either may not be minimum melting point material (which is true KRS-5) or may be more susceptible to attack by moisture. Further studies are needed to determine the exact nature of this effect.

During this past year, we have made our first fiber-loss measurements at 5.3 μm using a CO laser as a source. The values of α_T obtained in these measurements were always less than the corresponding values measured at 10.6 μm. Our results, shown in Table 2 for KRS-5 fiber (lengths ranged between 85 and 100 cm), indicate that the best fiber is actually only one-half as transparent at 5.3 μm as it is at 10.6 μm. In general, the losses are rather high at 5.3 μm. The lowest loss is about 3 dB/m, but most of the fibers have losses near 9 dB/m.

The most likely explanation for the higher loss at CO laser wavelengths is increased scattering. Table 3 gives the increase in α_T that would be expected if all of the extra loss at 5.3 μm were due to Rayleigh-type scattering mechanisms (varies as λ^{-4}). These data, which are normalized to 10.6 μm, indicate that the scattering loss at 5.3 μm would be expected to be 16 times greater than at 10.6 μm. But we observed, as Table 2 shows, lesser increases. Therefore, we conclude that the excess loss at 5.3 μm is not due to λ^{-4}-type scattering alone. Impurities in the material are another likely cause. Our future experiments will separate α_S and α_A at 5.3 μm and help us determine the precise nature of the 5.3-μm losses.

We have used two methods to measure the attenuation coefficient due to scattering (α_S). One method uses an integrating sphere to detect the total scattered light at the laser wavelength of interest. The other technique measures the RB spectrum using a Fabry-Perot interferometer and an Ar^+ laser as a source. Using the integrating or scattering sphere, we determine α_S for our KRS-5 fibers at 10.6 μm. With this

Table 2. Insertion Loss at 5.3 and 10.6 μm in KRS-5 Fiber

Fiber No.	Fiber Diameter, μm	Length, cm	Fiber Loss in dB/m at	
			5.3 μm	10.6 μm
108.6	500	100.0	8.03	4.24
108.5	500	103.5	2.98	1.01
107.1	500	105.0	3.44	0.72
107	400	99.0	12.1	2.24
109	250	95.5	11.6	1.17
110-11	250	108.0	16.1	2.79
110-10	250	105.0	8.56	4.20
112.1	250	87.5	10.1	1.94
110-9A	250	101.0	11.2	2.62
110-9C	250	101.0	7.53	2.51
114-4	250	97.0	8.65	1.79
111-21	250	102.5	7.32	1.44

7282

Table 3. Rayleigh-type (λ^{-4}) Scattering Losses at IR Laser Wavelengths (normalized to CO_2 laser wavelengths)

λ, μm	λ^{-4}, μm^{-4}	$\frac{(10.6)^4}{\lambda^4}$
10.6	7.92×10^{-5}	1
5.3	1.27×10^{-3}	16.0
3.8	4.80×10^{-3}	60.6
2.8	1.63×10^{-2}	206

7282

information and the insertion loss data (α_T), we determine the absorptive contribution, α_A (= $\alpha_T - \alpha_S$). The RB spectra enable us to study details of the Rayleigh scattering spectrum (normalized to the Brillouin scattered light) and thus, in principle, to isolate the various scattering mechanisms.

The integrating sphere has been used to measure scattered light in conventional silica fibers.[12] We have adopted some of these same techniques for our IR fibers, the only difference being that IR components are used. The sphere itself is 2.5 cm in diameter and coated on the inside with diffuse gold. A pyroelectric detector with a built-in op-amp detects and amplifies the signal obtained from the light scattered out of that portion of the fiber contained in the sphere. Generally, the scattered light signal is a few tenths of milliwatts with an incident power of 100 to 500 mW. In the actual measurements, the sphere is placed at the input end of the fiber and then moved every 2.5 cm to the output end for a complete set of scattering losses. Figure 12 illustrates the type of scattering data obtained from the point-by-point (differential light scattering) analysis just described. For this fiber, the scattered light decreases from the input end toward the middle of the fiber, as expected. The increased scattering at the 20-cm point is a hot spot of unknown origin (likely due to a structural change or impurity). The large scattering signal at the output end of the fiber, however, is rather unexpected. We have observed this behavior to varying extents in every fiber studied. The explanation is related in part to the finish on the end of the fiber. Figure 12 also shows data for two different end finishes on the same fiber. The standard finish was prepared by rubbing the end of the fiber with polishing paper (alumina-grit-impregnated paper), the hot-forged finish by pressing the end of the fiber against a hot tungsten carbide plate. Figure 12 shows that less light is scattered by the hot forged ends, although scattering is still strong. From these and similar data, we have found that the finish on the output end affects the amount of light scattered. In addition, we feel that the excess scattering occurring at this end results from higher-order modes. Since we do not strip these modes (mode stripping

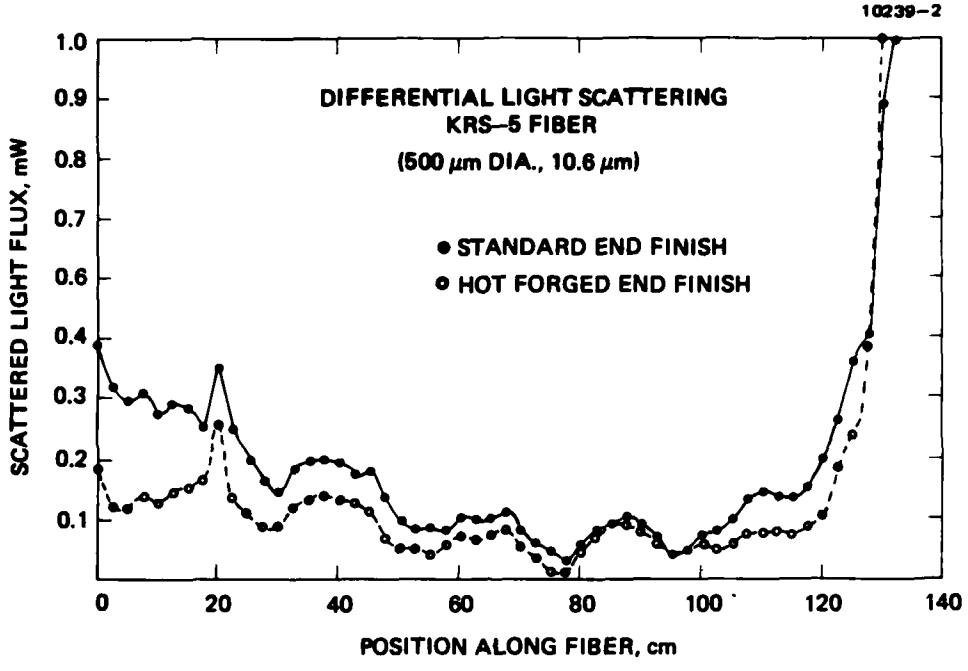

Figure 12. Scattering sphere measurements on KRS-5 fiber at 10.6 μm.

is virtually impossible at these high refractive indices), we have the possibility of propagating higher-order modes, which generally are quite lossy. Future experiments will be made to separate the contribution of the finish on the fiber end from that of higher-order modes.

The attenuation coefficient due to scattering α_S can be calculated from data such as given in Figure 12 and values of α_T as determined in the insertion-loss measurements. The amount of light scattered from a length dx of fiber at a distance x from the input end is given by

$$dI_S(x) = -I(x)\alpha_S dx \quad , \tag{1}$$

where $I(x) = I_o \exp(-\alpha_T x)$, and I_o is the incident intensity. In Eq. 1, an exponential decay of the scattered light signal is assumed. Integrating Eq. 1 from x_1 to x_2 gives the amount of light scattered from the fiber in this length:

$$\Delta I_S = I_S(x_2) - I_S(x_1) = \frac{I_o \alpha_S}{\alpha_T} [\exp(-\alpha_T x_2) - \exp(-\alpha_T x_1)] \quad . \tag{2}$$

Setting ΔI_T equal to

$$I_o [\exp(-\alpha_T x_2) - \exp(-\alpha_T x_1)]$$

yields (from Eq. 2) the following ratio:

$$\frac{\alpha_S}{\alpha_T} = \frac{\Delta I_S}{\Delta I_T} \quad .$$

Solving for α_S, we have simply

$$\alpha_S = \alpha_T \frac{\Delta I_S}{\Delta I_T} \quad . \tag{3}$$

A similar relationship exists for α_A when the subscript S is replaced by A in Eq. 3. These relationships indicate the expected proportionality between the attenuation coefficients and the respective light intensities. We have used Eq. 3 to determine α_S for several different KRS-5 fibers; α_A was then computed from $\alpha_A = \alpha_T - \alpha_S$. Table 4 lists the results obtained for α_T, α_S, and α_A at 10.6 μm.

The data generated by moving the integrating sphere along the fiber (see Figure 12) can be integrated using Eq. 3 to obtain an average α_S for the whole fiber (from $x_1 = 0$ to $x_2 = L$, where L is the length of the fiber). The integrated scattering intensity can then be plotted as a function of position along the fiber by adding the intensities point-by-point from $x_2 = L$ to $x_1 = 0$. These data, shown in Figure 13, are based on the data in Figure 12. Structure is absent in the integrated data of Figure 13 (hot spots are smoothed out in the integration), and the expected exponential dependence is absent for the entire length of the fiber. Instead, Figure 13 shows that the intensity of scattered light decays exponentially only for the region x = 0 to x = 100 cm. The output "end" of the fiber (x = 100 to x = 135 cm) shows a region of higher loss. This, of course, is expected from the differential scattering data (Figure 12). The values of α_S calculated from Eq. 3 are given in Table 4. Because these values were calculated assuming a constant α_T, they should be regarded as average values.

Table 4. Attenuation Coefficients for KRS-5 Fiber at 10.6 μm

Fiber No.	Diameter, μm	Length, cm	α_T, dB/m	α_S, dB/m	α_A, dB/m	Comments
119-3	500	135	0.57	0.31	0.26	Standard end finish
			0.57	0.27	0.30	Hot-forged ends
114-6	500	100	2.72	1.02	1.70	Standard end finish
			2.40	1.08	1.32	Turned end for end
			1.97	0.443	1.53	Hot-forged end
117-3	500	200	2.04	0.911	1.13	Standard end finish
115-6	500	136	2.28	0.089	2.19	BDG material

7282

The attenuation coefficients given in Table 4 indicate that α_A is less than α_A, although the two are approximately equal in most cases. In one unusual case (No. 115-6), the scattering was very small. We attribute this to the different starting material (BDH). This material seemed softer (lower extrusion pressure) and therefore the surface of the fiber may have been better (less scattering). But otherwise, BDH KRS-5 proved ineffective because the fiber's transmission degraded (see Section 2.C) greatly in only a few days. The data in Table 4 lead us to conclude that improvements both in materials (which would affect α_S and α_A) and fabrication techniques (which would affect mainly α_S) are required to produce a better waveguide.

The other method used in studying scattering losses in fiber materials is to measure the RB spectra of transparent solids using a Fabry-Perot interferometer. We have measured the RB spectra of undoped and doped, polycrystalline and single-crystal bulk KCl to obtain information on the attenuation due to various scattering mechanisms in these ultrapure materials. We recently gave a preliminary account of this work at the Physics of Fiber Optics Meeting held at the annual American Ceramic Society Meeting (Chicago, Illinois, 28-30 April 1980). A paper summarizing this research, which was funded in part by RADC (Contract No. F19628-78-C-0109), is included as an appendix. This paper gives the background required for understanding the light-scattering data presented in this section.

During this past year, the light-scattering apparatus was upgraded to provide better signal detection and processing. Data handling, which previously had relied on a multichannel analyzer for storage and processing, was considerably improved by interfacing the photon counting electronics via a CAMAC system to an LSI-11 computer. This system was programmed to function as a multichannel scaler to accumulate photon counts over many scans of the spectrum. The accumulated spectrum was then displayed on an oscilloscope (or chart recorder) and analyzed for peak amplitudes, positions, widths and for estimated uncertainties. Besides being much more efficient and convenient than the Northern multichannel analyzer used previously, this system allowed more accurate

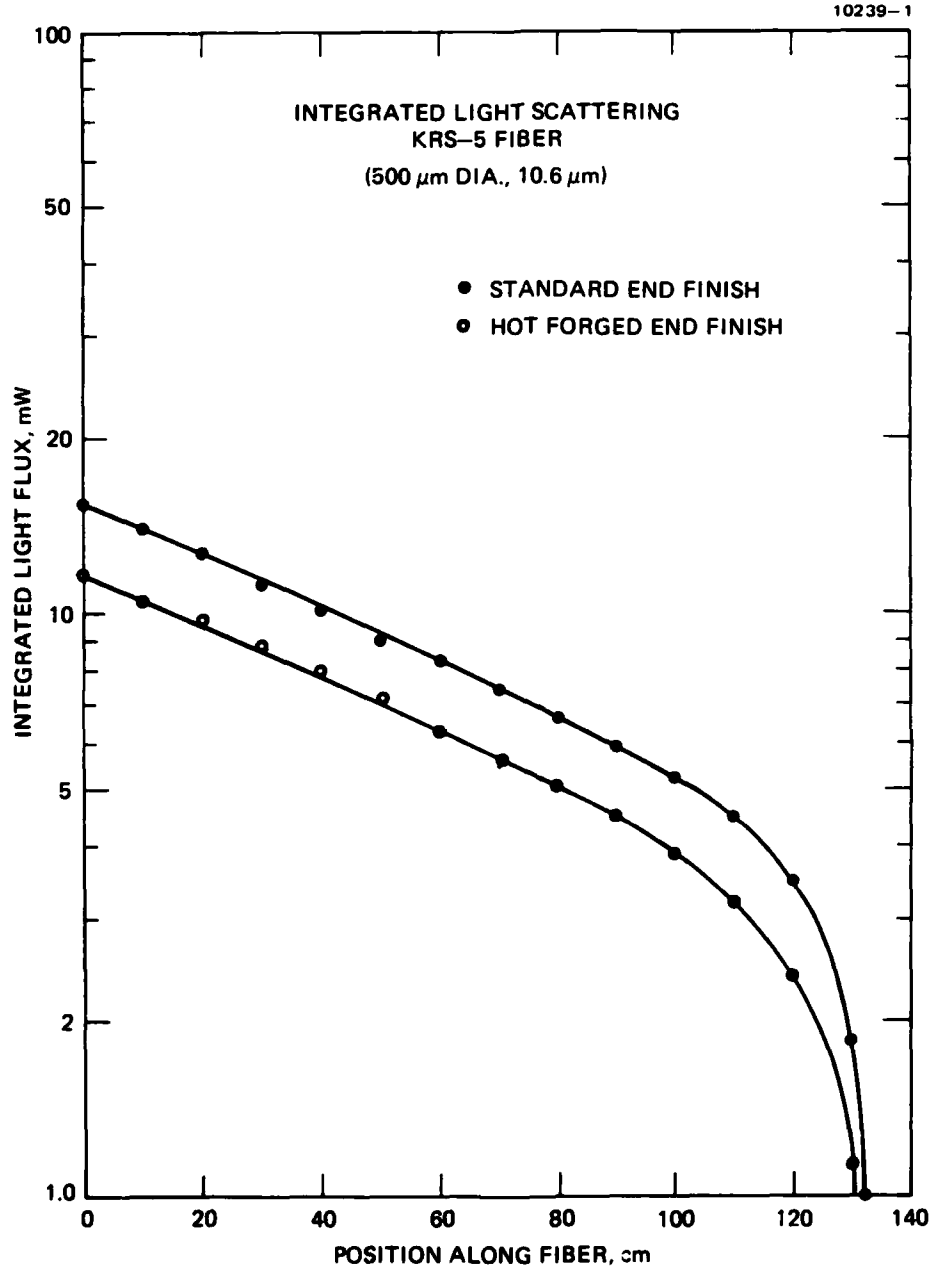

Figure 13. Integrated scattering data obtained from data in Figure 12.

calculations that would have been too tedious to perform before. For example, peak amplitudes may be determined by averaging over the peak width. This minimizes statistical fluctuations and errors due to the discreteness of the channels.

A 5-pass corner cube arrangement was implemented on our Fabry-Perot interferometer for comparison with the 3-pass arrangement that we normally use. Results on a crystalline KCl sample for equal run times and laser powers indicate that although the 5-pass system has, as expected, a higher contrast ratio, its lower throughput and S/N makes this modification unnecessary. Although a 5-pass system should theoretically yield a higher instrument finesse than a 3-pass system, we found the opposite to be true, probably because it is more difficult to stabilize the Fabry-Perot plates when the light signal is smaller. We conclude that the 3-pass corner cube arrangement is preferred for these studies.

The data obtained on undoped, polycrystalline KCl are summarized in Table 5. Four polarizations were studied, and the Rayleigh (I_R) and Brillouin (I_B) scattered light intensities are given for each configuration. From these intensities, the Landau-Placzek ratios (R_{LP}, which is equal to $I_R/2I_B$) were calculated. In general, the scattering was greater in polycrystalline KCl than in single-crystal KCl. Also, the sound velocity (V_S) data in Table 5 show that there are three distinct Brillouin lines. The highest velocity matches the longitudinal mode observed in single-crystal KCl, while the lower velocities most likely correspond to mixed modes that are both longitudinal and transverse in character. The Krishnan ratio, $\rho_h \equiv I_R(VH)/I_R(HH)$, was found to be 0.384 for this sample. This ratio is theoretically predicted to be 1, but for most materials it is less than 1. We hope that a study of ρ_h will help us identify the various Rayleigh scattering mechanisms. At this time, however, we do not have an interpretation for ρ_h.

Table 6 gives, as a consistency check, data on a crystalline sample that had been run six months earlier. Over this period, changes in the system included new photon counting electronics, collection and collimation lenses, and plate spacing. These changes are expected to affect the absolute amplitudes of the peaks, but one anticipates that the

Table 5. Data for Polycrystalline KCl B150

Polarization	I_R	I_B	R_{LP}	V_S,
	Hz/W of Incident Power			m/sec
VV	1.36×10^6	3080	220	2650
		19900	34	3941
VH	1.57×10^5	78.6	998	2360
		99.8	787	3960
HV	1.67×10^5	292	285	2679
		810	103	3950
HH	4.09×10^5	349	586	2353
		317	644	2662
Krishnan ratio $\rho_h = 0.384$				

Table 6. Data for Crystalline KCl B153

Date	Polarization	I_R	I_B	R_{LP}	V_S,
		Hz/W of Incident Power			m/sec
8 Aug 80	VV	8.81×10^5	18000	24	4021
	VH	5.16×10^4	1160	22	1823
	HV	4.12×10^4	901	23	1841
	HH	1.81×10^5	271	334	4009
	$\rho_h = 0.285$				
8 Feb 80	VV	2.46×10^6	12900	95	3669
	VH	4.54×10^4	991	23	1676
	HV	5.29×10^4	861	31	1706
	HH	1.99×10^5	332	300	3680
	$\rho_h = 0.228$				

ratios R_{LP} and ρ_h will be fixed properties of the sample. The agreement between the two runs is reasonably good, with the notable exception of the VV polarization. We noted that, by adjusting the sample position, the VV Rayleigh peak varied, while the Brillouin peak was constant to within ±7%. Since an R_{LP} as large as 147 could be obtained this way, this could account for the large R_{LP} of the earlier run.

To investigate further this variation in Rayleigh scattering, we studied a crystalline KCl sample cut in a (100)-oriented parallelopiped with dimensions of 10 x 10 x 38 mm. If scattering from the surfaces of the sample contributes to the Rayleigh peak in the spectrum, this contribution should be distinguished by a dependence on geometric factors such as the path length of the laser beam inside the sample. Table 7 summarizes data for positions of the sample oriented to give a short or long path length. For each position, the sample was first translated to a spot where the Rayleigh peak was at a minimum. The table shows that the scattering was slightly lower for the shorter path length. Then the sample was translated parallel to the beam a distance of about 1 mm until the Rayleigh peak was at a maximum. Moving the sample in this way kept the points on the surface where the beam enters and exits from moving. The table shows that, for VV, this approximately doubled I_R. The sample was then translated transverse to the beam so that the beam hits different spots on the surface. We should expect the variation of I_R to be larger in this case, since the beam might hit dust or defects on the surface. And for VV, Table 7 does indeed show a maximum I_R that is about 20% larger than for parallel translation. But for V_H, the trends are not clear, possibly due to the difficulty in trying to minimize or maximize a very small signal. This topic deserves further investigation, perhaps comparing large and small pieces cut from the same sample.

A major emphasis in our future light-scattering studies will be on the nature and source of the Rayleigh-scattered light. To obtain meaningful and readily interpretable Rayleigh data, we have selected matched sets of single and polycrystalline KCl (doped and undoped) for extensive study. These samples are matched by selecting polycrystalline and single-crystal samples made from the same KCl ingot. Table 8 lists

Table 7. Rayleigh Variation in Crystalline KCl B169-1A

Polarization	Path Length, mm	I_R min	I_R max (∥)	I_R max (⊥)	I_B avg
		Hz/W Incident Power			
VV	10	62300	123000	153000	2660 ± 80
	38	73500	145000	168000	2170 ± 120
VH	10	2590	3220	3340	147 ± 7
	38	3180	5500	3920	128 ± 3

Table 8. KCl Samples for Light-Scattering Studies

Sample No.	Structure[a]	Forging Conditions	Dopant Concentration	Orientation
35	S	--	--	(100) ± 2
59	P	71.8%, 250°C	--	Rectangular
115-3	S,P	--	Eu^+, 500 ppm	(100)
127-3	S,P	65%, --	SR^{++},100 ppm	(100)
150-1	S,P	68%, --	--	(100)
151-3	S,P	68.3%, --	--	(100)
153	S	--	--	(100)
154-5A	S,P	60.9%, 250°C	--	(100)
156-5	S,P	71.8%, 280°C	Rb^+, 0.75%	(100)
158-3	S	--	Rb^+, 1.75%	(100)
164	S,P	67.1%, 300°C	Rb^+, 1.75%	(100)
166	S	--	Rb^+, 0.75%	Cylinder
167-6	S,P	68.4%, 300°C	--	(100)
169-1A	S	--	--	(100)
179	S	--	--	Twinned, rectangular

[a]S = single crystal, P = polycrystalline.

these materials, the dopants, amount of hot forging, and crystal orientation. We will measure the scattering intensities in these materials at room temperature and as a function of temperature. At elevated temperatures, we would expect the impurities to move and thus the intensities of the Rayleigh scattered light to change. Other measurements planned to delineate elastic scattered light mechanisms include studies of the dependence of the scattered light on frequency and on scattering angle.

SECTION 3

FUTURE PLANS AND RECOMMENDATIONS

During the first year of research in low-loss fibers, we began to develop new fabrication techniques for preparing metal halide fibers. Next year, we will abandon extrusion techniques for the alkali halides in favor of (1) single-crystal fiber growth and (2) hot-rolling fibers. The first approach will be attempted as a means of producing the ultimate low-loss fiber, one essentially free of gross scattering centers such as grain boundaries. The single-crystal growth procedure will involve a closed crucible system for growing, at first, KCl fibers. The closed crucible will permit introducing RAP conditions to purify the melt as well as to grow KCl fibers. Fibers will be extruded from the melt through a quartz-orifice, which is used to provide the smooth surface and uniform diameter of the pulled fiber (RAP leads to minimal surface tension between the fiber and quartz surfaces). If the first short lengths ($\sim$25 cm) of fiber appear successful, the process will be modified to allow spooling the fiber (also under RAP conditions) for longer lengths. Other materials, including the thallium halides, may also be subjected to single-crystal growth once the system has been tested with KCl. The second approach uses hot-rolling to roll polycrystalline fibers. We will use our new rollers to provide a smoother, nonsticking surface for KCl. In addition to the alkali halides, some limited rolling will be done on the thallium halides.

A new area we wish to develop during the next year is cladding for our IR fiber. We propose to first study post-extrusion cladding techniques for KRS-5 fiber and later for single-crystal fibers. One method used to clad the fiber will be ion exchange. Specifically, the substitution $Br^- \rightarrow I^-$ in KRS-5 will be emphasized. This would provide a core (TlBrI) index of 2.37 and a clad (TlBr) index of 2.33. Our earlier studies showed that ion exchanging Cl^- for Br^- and I^- in KRS-5 led to a uniform-looking cladding, but that the transmission was poor. These studies were terminated before a thorough analysis had been done, and we now feel that the $Br^- \rightarrow I^-$ exchange may lead to a fiber with better

optical quality. Ion exchange will be attempted using liquid (e.g., HBr) and gas phase chemistry on extruded KRS-5 fiber.

The fiber developed, both clad and unclad, will be evaluated optically using insertion-loss and scattering measurements. Insertion-loss measurements will be carried out at 3.8, 5.2, and 10.6 μm. Scattering measurements will be made using an integrating sphere and also our Brillouin scattering spectrometer for measurement of the RB spectra of bulk and fiber materials. Grain boundary scattering will continue to be emphasized, and theories will be sought to correlate the optical and structural properties of our fibers. Additional analytic facilities, such as an SEM (for index profiling and general structural features), laser calorimetry (for absorption coefficient measurements on bulk materials), and Zeeman atomic absorption (for determination of impurity content) will be used as needed in the optical evaluation of our fibers.

REFERENCES

1. S. Kobayashi, N. Shibata, S. Shibata, and T. Izawa, "Characteristics of Optical Fibers in Infrared Wavelength Region," Rev. of Elect. Comm. Lab. (Japan) 26, 453-468, 1978.

2. L.G. Van Uitert and S.H. Wemple, "$ZnCl_2$ Glass: A Potential Ultralow-Loss Optical Fiber Material," Appl. Phys. Lett. 33, 57-59, 1978.

3. M. Robinson, R.C. Pastor, R.R. Turk, D.P. Devor, M. Braunstein, and R. Braunstein. "Infrared-Transparent Glasses from the Fluorides of Zirconium, Thorium, and Barium," Mat. Res. Bull. 15, 735-742, 1980.

4. M. Poulain, M. Chanthanasinh, and J. Lucas, "New Fluoride Glasses," Mat. Res. Bull. 12, 151-156, 1977.

5. S. Mitachi and T. Manabe, "Fluoride Glass Fiber for Infrared Transmission," Jap. Journal of Appl. Phys. 19, L313-L314, 1980.

6. D.A. Pinnow, A.L. Gentile, A.G. Standlee, A.J. Timper, and L.M. Hobrock, "Polycrystalline Fiber Optical Waveguides for Infrared Transmission," Appl. Phys. Lett. 33, 28-29, 1978.

7. A.L. Gentile, M. Braunstein, D.A. Pinnow, J.A. Harrington, D.M. Henderson, L.M. Hobrock, J. Myer, R.C. Pastor, and R.R. Turk, "Infrared Fiber Optical Materials," in Fiber Optics: Advances in Research and Development, ed. by B. Bendow and S.S. Mitra, Plenum Publishing, N.Y., pp. 105-118 (1977).

8. J.A. Harrington, "Infrared Fiber Optics for CO_2 Laser Applications," in CO_2 Laser Devices and Applications, Proceedings of SPIE Technical Symposium East, Vol. 227, Fall 1980.

9. D. Chen, R. Skogman, G.E. Bernal, and C. Butter, "Fabrication of Silver Halide Fibers by Extrusion," in Fiber Optics: Advances in Research and Development, ed. by B. Bendow and S.S. Mitra, Plenum Publishing, N.Y. pp. 119-122 (1977).

10. S.D. Allen and J.A. Harrington, "Optical Absorption in KCl and NaCl at Infrared Laser Wavelengths," Appl. Opt. 17, 1679-1680, 1978.

11. R.C. Pastor and A.C. Pastor, "Crystal Growth in a Reactive Atmosphere," Mat. Res. Bull. 10, 117-124, 1975.

12. A.R. Tynes, A.D. Pearson, and D.L. Bisbee, "Loss Mechanisms and Measurements in Clad Glass Fibers and Bulk Glass," J. Opt. Soc. Amer. 61, 143-153, 1971.

APPENDIX

SCATTERING LOSSES IN SINGLE AND POLYCRYSTALLINE MATERIALS FOR INFRARED FIBER APPLICATIONS

J.A. Harrington and M. Braunstein

Hughes Research Laboratories†

Malibu, CA 90265

B. Bobbs* and R. Braunstein

University of California at Los Angeles††

Los Angeles, CA 90024

ABSTRACT

Polycrystalline fiber waveguides, fabricated from infrared transparent solids such as KRS-5 and KCl, have measured losses much greater than conventional silica fibers. One major source of these losses is scattering from grain boundaries present in the polycrystalline fibers. To improve the optical transmission of our infrared waveguides, we have studied the losses due to scattering in single and polycrystalline materials which are suitable for fabrication into infrared transmissive waveguides.

*Hughes Staff Doctoral Fellow.

†This work has been supported by Hughes Aircraft Company internal research and development programs and by RADC, Hanscom AFB, Mass.

††This work has been supported in part by AFOSR and ARO (Durham).

INTRODUCTION

Optical fiber waveguides made from crystalline materials such as KRS-5 (TlBrI), TlBr, AgCl, and KCl have been used for a variety of 10.6-μm, CO_2 laser applications.[1-4] The losses in the current IR fibers, however, are high (lowest loss measured is 300 dB/km at 10.6 μm in KRS-5) and applications in sensor and laser power delivery systems have been limited to short (1- to 2-m) lengths of fiber.[2-4] This measured IR fiber attenuation is considerably higher than that predicted theoretically for these and related IR transparent materials.[2,5] In fact, Gentile et al.[2] and van Uitert and Wemple[5] have shown that these materials have projected losses as low as 10^{-3} dB/km near 5 μm. To develop this ultra-low-loss potential, for such applications as long-distance communication links, requires a careful analysis of the nature of the attenuation mechanisms present in IR transparent waveguides. In this paper, we address the contribution of scattering to the total attenuation in bulk materials that have the potential for being fabricated into highly transparent fibers.

The attenuation mechanisms present in low-loss solids are illustrated in Fig. 1 for fused silica. At the shortest wavelengths, electronic processes (Urbach tail) contribute heavily to the total loss. At the IR wavelengths of interest, however, two mechanisms — scattering and multiphonon absorption — have been identified as the ultimate, limiting loss processes.[2] In Fig. 1, the curves for

scattering (which decreases as λ^{-4} with increasing wavelength) and lattice (multiphonon) absorption (which increases exponentially with increasing wavelength) cross to yield a minimum in the total attenuation. For fused silica, this minimum, which is about 0.25 dB/km at 1.6 μm, has been achieved in kilometer-long fibers.[6] For certain crystalline as well as special glassy solids, minima occur near 5 μm with projected losses well below the intrinsic losses measured in silica (projected losses are given in the next section).

The total attenuation coefficient α_T may be written as the sum

$$\alpha_T = \alpha_S + \alpha_A \quad , \tag{1}$$

where α_S and α_A are the contributions due to scattering and absorption, respectively. Each term in Eq. 1 can be measured independently, thus allowing the individual mechanisms contributing to the overall optical loss in solids to be studied. For example, α_T can be obtained from standard spectroscopic and fiber insertion loss measurements while laser calorimetry has been used very successfully to determine residual absorption α_A in weakly absorbing materials. The scattering terms α_S has not been as well studied. Measurements using integrating spheres for both bulk and fiber materials are generally used to obtain a total integrated scattering (TIS) loss.

These methods, however, have the disadvantage of being unable to distinguish among the various individual scattering mechanisms contributing to TIS. To elucidate the various scattering mechanisms as well as to obtain a value for α_s, we have chosen to study the light scattering spectra of solids. These spectra are composed of elastically (Rayleigh) scattered light that results from various nonpropagating fluctuations in the materials index of refraction and inelastically (Brillouin) scattered light that results from the interaction of light and the thermal motion of ions (sound waves). Although Rayleigh-Brillouin (RB) spectra have been used to measure α_s in glasses,[7] this technique has not been expressly used before to study scattering losses in single- and poly-crystalline materials. In this work, we have measured RB scattering at 90° in bulk single- and poly-crystalline KCl. As discussed in the next section, we expect very little Rayleigh scattering in single-crystal materials; for polycrystalline samples, however, intuition suggests that the residual strain and grain boundaries associated with the hot press-forged, polycrystalline material should lead to larger amounts of scattering. Our preliminary results support this presumption, but we have not yet been able to account for the source of each scattering mechanism contributing to the RB spectra.

GENERAL CONSIDERATIONS

The limiting attenuation mechanisms in transparent solids are scattering and multiphonon absorption. These contributions have

been considered by several investigators in the context of projecting future ultra-low-loss materials for the next generation of fiber waveguides. Van Uitert and Wemple[5] have studied the potential of $ZnCl_2$ (a glass former) while Gentile et al.[2] and Pinnow et al.[1] have concentrated on the crystalline materials. In Fig. 2, we consider the projected transmission for KRS-5 and KCl and compare these predictions to fused silica. The curves in Fig. 2 show the characteristic V shape resulting from the crossing of the scattering (short wavelength) and multiphonon (long wavelength) attenuation mechanisms. The only scattering mechanism assumed in calculating the λ^{-4}-dependent scattering curve for KRS-5 and KCl was Brillouin scattering (α_B - see below). As mentioned above, the V-shaped curve for silica has essentially been traced out experimentally and thus silica fiber losses are now intrinsic. For KCl and KRS-5 (as well as for many other non-oxide ionic solids), however, Fig. 2 shows the extremely low loss potential for these materials near 5 μm.

To determine α_S from RB light scattering experiments requires a careful measurement of the intensity of both the Brillouin- and Rayleigh-scattered light. Brillouin scattering results from light that has been inelastically scattered (Bragg scattering) from acoustical phonons (sound waves). The frequency of the scattered light is Doppler shifted from the frequency of the laser light ω_L by an amount $\pm\Omega$:

$$\Omega = \frac{4\pi n V \sin(\theta/2)}{\lambda_o} \quad ,$$

where n is the index of refraction of the medium, v is the velocity of sound, θ is the scattering angle, and λ_o is the vacuum wavelength of the light. This frequency shift has been well studied in alkali halides.[8] The Rayleigh-scattered light (central maximum at ω_L) is due to scattering of light from nonpropagating fluctuations in the dielectric constant. In glasses, mechanisms which give rise to these fluctuations include: density variations resulting from the frozen-in, random variations in dielectric constant inherent in a disordered solid; concentration fluctuations resulting from the local compositional variations present in mixtures; and entropy fluctuations resulting from temperature variations.[7] Of the three, only entropy fluctuations, which are very weak, would be present in an ideal single crystal.

To obtain α_S, we first evaluate the intensity ratio of the Rayleigh (I_R) to the total Brillouin ($2I_B$) scattered light. This ratio is called, based on its use in light scattering in liquids, the Landau-Placzek ratio R_{LP} and is defined[7] as

$$R_{LP} \equiv \frac{I_R}{2I_B} \quad . \qquad (2)$$

Strictly speaking, since I_R and thus R_{LP} are related to specific scattering mechanisms (such as those discussed above for glasses),

measured values of R_{LP} are generally regarded as a property of a given material (e.g., fused SiO_2 has an $R_{LP} \simeq 23$, while $33K_2O\text{-}67SiO_2$ has an $R_{LP} \simeq 10$).[9] In our experiments, we measure I_R without, in general, knowing the specific mechanisms contributing to the Rayleigh component of scattered light. Therefore, we should more appropriately speak of an effective Landau-Placzek ratio with I_R representing the intensity of the central maximum.

The measured R_{LP} is then used to calculate α_S, as described by Pinnow et al.[10] and others,[7,9] from the relationship

$$\alpha_S = \alpha_B(R_{LP} + 1) \quad , \tag{3}$$

where α_B, is the small residual attenuation coefficient due to Brillouin scattering alone. It is given by

$$\alpha_B = \frac{8\pi^3}{3} \frac{1}{\lambda_o^4} (n^8 P_{12}^2)\, k_B\, T B_T \quad , \tag{4}$$

where P_{12} is the photoelastic (Pockels) coefficient, T is the temperature, k_B is Boltzmann's constant, and B_T is the isothermal compressibility. For ideal single crystals, $I_R \simeq 0$, thus $R_{LP} \simeq 0$ and (from Eq. 3) $\alpha_S \simeq \alpha_B$. This leads to the scattering curves in Fig. 2 for KRS-5 and KCl, which were calculated from Eq. 4 alone, while the scattering for fused silica was calculated from Eq. 3 using $R_{LP} = 23$.

An interesting feature of measured R_{LP}s for crystalline solids is their dependence on polarization. For our single-crystal measurements in KCl, a [100] crystal orientation was used for most samples studies. With incoming light along the [100] direction and scattered light along the [010], the polarization of the incident and analyzed scattered light was either vertical (V) or horizontal (H) with respect to the scattering plane. For this geometry, we may determine the intensities of the Brillouin components from the selection rules for the rock salt structure (O_h) and the differential cross section.[11] The intensities I and allowed vibrational modes for the various polarizations (phonon momentum q along [110] direction) are summarized in the matrix given in Table 1a. Using the known photoelastic (P_{12} and P_{44}) and elastic (C_{11}, C_{12}, and C_{44}) constants for KCl,[12] we calculate the matrix elements in Table 1a and give them, normalized to I_{HH} (the weakest intensity), in Table 1b. Table 1b shows that the intensities of the longitudinal modes (frequency equal to 15.8 GHz) in VV polarization are much stronger than those in the other polarizations (transverse mode frequency equal to 7.2 GHz). This means that measured Landau-Placzek ratios may vary greatly depending on crystal orientation and polarization, with the smallest R_{LP} occurring for the VV polarization.

LIGHT SCATTERING MEASUREMENTS

The RB spectra were recorded using as a source an Ar-ion laser (Spectra Physics Model 165) delivering 10 to 300 mW of single-line power and a PZT-scanned Fabry-Perot spectrometer. The experimental set-up is shown in the block diagram in Fig. 3. The spectrometer is a Burleigh Instruments, Inc., actively stabilized Fabry-Perot interferometer with its associated photon counting electronics. Data acquisition is provided by a 512-channel Tracor-Northern multichannel analyzer (MCA). This MCA has proven essential for obtaining good S/N ratios for these crystals (between 2000 and 20,000 scans are generally accumulated for each spectrum).

To improve the contrast of the spectrometer, we added a three-pass attachment to the interferometer. This allowed us to readily detect the Brillouin components in the polycrystalline materials where the Rayleigh scattering is more intense. Fig. 4 shows the results of a 90° scattering measurement on polycrystalline KCl doped with 1.75% RbCl taken with the light passing once (one-pass) or thrice (three-pass) through the interferometer. The improved contrast in the three-pass case is obvious. Note in particular the resolution of the transverse modes in the three-pass case that has been lost in the Rayleigh wing in the one-pass case. Clearly, the three-pass arrangement, which has been used in all our measured data, is necessary to obtain a reliable R_{LP}. The resolution of the triple-pass Fabry-Perot spectrometer was 0.03 cm^{-1} (finesse equal to 50).

RESULTS OF LIGHT SCATTERING EXPERIMENTS

Measurements of scattering losses were made at 488.0 nm in bulk single and polycrystalline KCl. The KCl was reactive atmosphere process (RAP) single-crystal material[13] which was either used in oriented single-crystal (SC) or in hot-press forged, polycrystalline (P) form. The RB scattering data shown in Fig. 5 are for pure, single-crystal KCl oriented as shown in the insert. From the data, we can see the intense stokes (S) and anti-stokes (AS) longitudinal Brillouin components in the VV polarization. The Brillouin components are also seen to become weaker in VH (or HV) and HH polarization, which is in qualitative agreement with the results stated in Table 1 for this scattering geometry. Similar results were obtained for other RAP-grown KCl (SC) although the R_{LP}s were found to vary somewhat from sample to sample.

The data for polycrystalline KCl (average grain size, 10 μm) are shown for two polarizations in Fig. 6. We can see from these data the intense Rayleigh scattering typical of our polycrystalline samples. In this sample, we also note the presence of only longitudinal modes in VV polarization and transverse modes in VH polarization. This leads us to conclude that we have, by chance, illuminated an axis of high symmetry in this sample. Specifically, it would appear from the data that the crystallites are oriented along the [100] direction for this particular experiment. In general, we would expect to observe an admixture of L and T modes

consistent with a random orientation of polycrystalline samples.

Effective Landau-Placzek ratios have been calculated for these two samples from the data in Figs. 5 and 6. These data are summarized in Table 2. For the single-crystal KCl, R_{LP} is lowest for the VV polarization, as discussed above, but the R_{LP}s for other polarizations do not scale with the predicted Brillouin intensities (see Table 1). This is due to the polarization dependence of the Rayleigh-scattered light. Our measurements of I_R indicate that the Rayleigh scattered light is, as expected, most intense for the VV polarization. For this polarization, I_R is approximately 8 to 10 times stronger than when measured under HV, VH, or HH conditions. More detailed studies of the depolarization ratio might give insight into the nature of the static defect contribution to elastic scattering. In general, the values for R_{LP} obtained for polycrystalline KCl(P) are higher than those for KCl(SC) (see Table 2). Again, the VV polarization for this unoriented poly sample yields the lowest R_{LP} and the HH case yields the highest R_{LP} (this trend was also seen in another KCl(P) sample).

Table 2 also gives the values of α_S calculated from Eqs. 3 and 4, which, for KCl at 488.0 nm, reduce to,

$$\alpha_S = 1.5 \times 10^{-6} \, (R_{LP} + 1) \ \mathrm{cm}^{-1} \quad .$$

These attenuation coefficients due to scattering may be compared to the absorption coefficients obtained for KCl by laser calorimetric measurements at 488.0 nm by Harrington et al.[14] They found $\alpha_A \tilde{=} 3 \times 10^{-4}$ cm^{-1} for KCl(P) and $\alpha_A < 2 \times 10^{-5}$ cm^{-1} for KCl(SC). We see, therefore, that the total attenuation $\alpha_T (= \alpha_A + \alpha_S)$ is largely due to scattering.

The nature of the Rayleigh scattering in our crystalline samples is not completely understood. The results indicate substantial elastic scattering beyond that predicted above theoretically from entropy fluctuations. One may consider this excess parasitic scattering as arising from mechanical and chemical defects in the crystal. Although all the KCl has been RAP purified, we cannot rule out different amounts of chemical impurities in each sample. It is also evident that residual strain is present in both single and polycrystalline samples (observed as birefringence in crossed polarizers). This strain, which one would intuitively expect to be greater in the hot-forged polycrystalline materials, can lead to substantial elastic scattering. In particular, one would suspect grain boundaries as a potentially strong source of Rayleigh scattering because impurities, voids, and high strain would be more prevalent in these areas.

In our polycrystalline samples, it was not possible to examine the scattering from a single grain boundary because the average grain size (10 μm) was much smaller than the scattering volume

(cylindrical volume, 350 μm long by 30 μm in diameter). Brody et al.,[15] however, were able to study elastic scattering from a single grain boundary in polycrystalline calcium fluoride (Irtran-3). In their measurements, the grain size (150 μm) was larger than the scattering volume and they found essentially no difference in the intensity of light scattered from within a crystallite to that scattered from a volume containing a grain boundary. One might conclude from their results that grain boundaries do not contribute to elastic scattering; however, to assess the effect of grain boundaries properly, one must study high-purity material with a low Rayleigh background. Our future experiments will look more closely at the effect as well as the importance of residual strain on the Rayleigh scattered light.

SUMMARY

Our RB scattering studies on bulk KCl have been an initial attempt to probe the mechanisms responsible for scattering losses in highly transparent materials. We have found that polycrystalline materials scatter more strongly than do single-crystal materials, but we have not as yet been able to explicitly associate a particular elastic scattering process with a finite contribution to the total scattering. Our results, however, do indicate that, even in these very pure KCl samples, there is more scattering than predicted for the ideal KCl crystals and thus future fiber waveguides from these low-loss materials may be limited

more by scattering than absorption losses. Consequently, it is important to study scattering in poly- and single-crystal materials to understand the origin of the Rayleigh scattering and thereby to determine methods of minimizing this contribution to the attenuation.

REFERENCES

1. D.A. Pinnow, A.L. Gentile, A.G. Standlee, A.J. Timper, and L.M. Hobrock, "Polycrystalline Fiber Optical Waveguides for Infrared Transmission," Appl. Phys. Lett., Vol. 33, pp. 28-29, 1978.
2. A.L. Gentile, M. Braunstein, D.A. Pinnow, J.A. Harrington, D.M. Henderson, L.M. Hobrock, J. Myer, R.C. Pastor, and R.R. Turk, "Infrared Fiber Optical Materials," in Fiber Optics: Advances in Research and Development, ed. by B. Bendow and S.S. Mitra, pp. 105-118, Plenum Publishing, N.Y., 1977.
3. D. Chen, R. Skogman, G.E. Bernal, and C. Butter, "Fabrication of Silver Halide Fibers by Extrusion," ibid, pp. 119-122.
4. J.A. Harrington, "Infrared Fiber Optics for CO_2 Laser Applications," in CO_2 Laser Devices and Applications, Proceedings of SPIE Technical Symposium East, Vol. 227, Fall, 1980.
5. L.G. Van Uitert and S.H. Wemple, "$ZnCl_2$ Glass: A Potential Ultralow-Loss Optical Fiber Material," Appl. Phys. Lett., Vol. 33, pp. 57-59, 1978.

6. S. Kobayashi, N. Shibata, S. Shibata, and T. Izawa, "Characteristics of Optical Fibers in Infrared Wavelength Region," Rev. of Elect. Comm. Lab. (Japan), Vol. 26, pp. 453-468, 1978.

7. For a review see J. Schroeder, "Light Scattering of Glass," in Treatise on Materials Science and Technology, Vol. 12 Glass 1: Interaction With Electromagnetic Radiation, pp. 157-222, Academic Press, 1977.

8. G.B. Benedek and K. Fritsch, "Brillouin Scattering in Cubic Crystals," Phys. Rev., Vol. 149, pp. 647-662, 1966.

9. J. Schroeder, R. Mohr, P.B. Macedo, and C.J. Montrose, "Rayleigh and Brillouin Scattering in K_2O-SiO_2 Glasses," J. Amer. Cer. Soc., Vol. 56, pp. 510-514, 1973.

10. T.C. Rich and D.A. Pinnow, "Total Optical Attenuation in Bulk Fused Silica," Appl. Phys. Lett., Vol. 20, pp. 264-266, 1972.

11. W. Hayes and R. Loudon, "Scattering of Light by Crystals, pp. 327-353, J. Wiley & Sons, 1978.

12. Landolt-Bornstein Numerical Data and Functional Relationships in Science and Technology, New Series, ed. by K.H. Hellwege and A.M. Hellwege, Vol. II, pp. 25, 29, 510, and 513, Springer-Verlag, 1979.

13. R.C. Pastor and A.C. Pastor, "Crystal Growth in a Reactive Atmosphere," Mat. Res. Bull., Vol. 10, pp. 117-124, 1975.

14. J.A. Harrington, B.L. Bobbs, M. Braunstein, R. Kim, R. Stearns, and R. Braunstein, "Ultraviolet-Visible Absorption in Highly Transparent Solids by Laser Calorimetry and Wavelength Modulation Spectroscopy," Appl. Opt., Vol. 17, pp. 1541-1546, 1978.

15. E. Brody, C. Roychoudhuri, and M. Hercher, "Brillouin Spectra of CaF_2 Microcrystals Using a Stable 3-Pass Fabry-Perot Interferometer," Appl. Phys. Lett., Vol. 23, pp. 543-545, 1973.

TABLE I

Intensities of Brillouin Components for a Rocksalt Crystal

(a)

Mode	I_{VV}	$I_{VH} = I_{HV}$	I_{HH}
(110) L	$\frac{4P_{12}^2}{C_{11} + C_{12} + C_{44}}$	0	$\frac{4P_{44}^2}{C_{11} + C_{12} + C_{44}}$
(1$\bar{1}$0) T	0	0	0
(001) T	0	$\frac{P_{44}^2}{2C_{44}}$	0

(b)

Mode	I_{VV}	I_{VH}	I_{HH}
(110) L	133	0	1
(1$\bar{1}$0) T	0	0	0
(001) T	0	4.8	0

TABLE II

Effective R_{LP} and Calculated Values of α_S

Structure	Polarization	R_{LP}	α_S (cm^{-1})
Single	VV	26.2	4.1×10^{-5}
Crystal	VH	38.5	5.9×10^{-5}
(SC)	HV	44.9	6.9×10^{-5}
	HH	276.4	4.2×10^{-4}
Polycrystalline	VV	496	7.5×10^{-4}
(P)	VH	830	1.2×10^{-3}
	HV	1598	2.4×10^{-3}
	HH	>5000	$>7.5 \times 10^{-3}$

FIGURE CAPTIONS

Fig. 1 - Schematic representation of optical attenuation mechanisms in solids.

Fig. 2 - Projected losses for some IR transparent materials. Short wavelengths are bounded by $1/\lambda^4$-scattering and long wavelengths by multiphonon absorption.

Fig. 3 - Block diagram of scanning Fabry-Perot interferometer for measuring RB spectra.

Fig. 4 - Improved contrast in RB spectra of poly KCl + 1.75% RbCl through the use of 3-pass attachment on Fabry-Perot interferometer. The spectra were all recorded using the 3-pass configuration.

Fig. 5 - Scattering spectra for single-crystal KCl for three different polarizations. Landau-Placzek ratios are given in Table 2 for these data.

Fig. 6 - Scattering spectra for polycrystalline KCl (average grain size is 10 μm). Landau-Placzek ratios are given in Table 2 for these data.

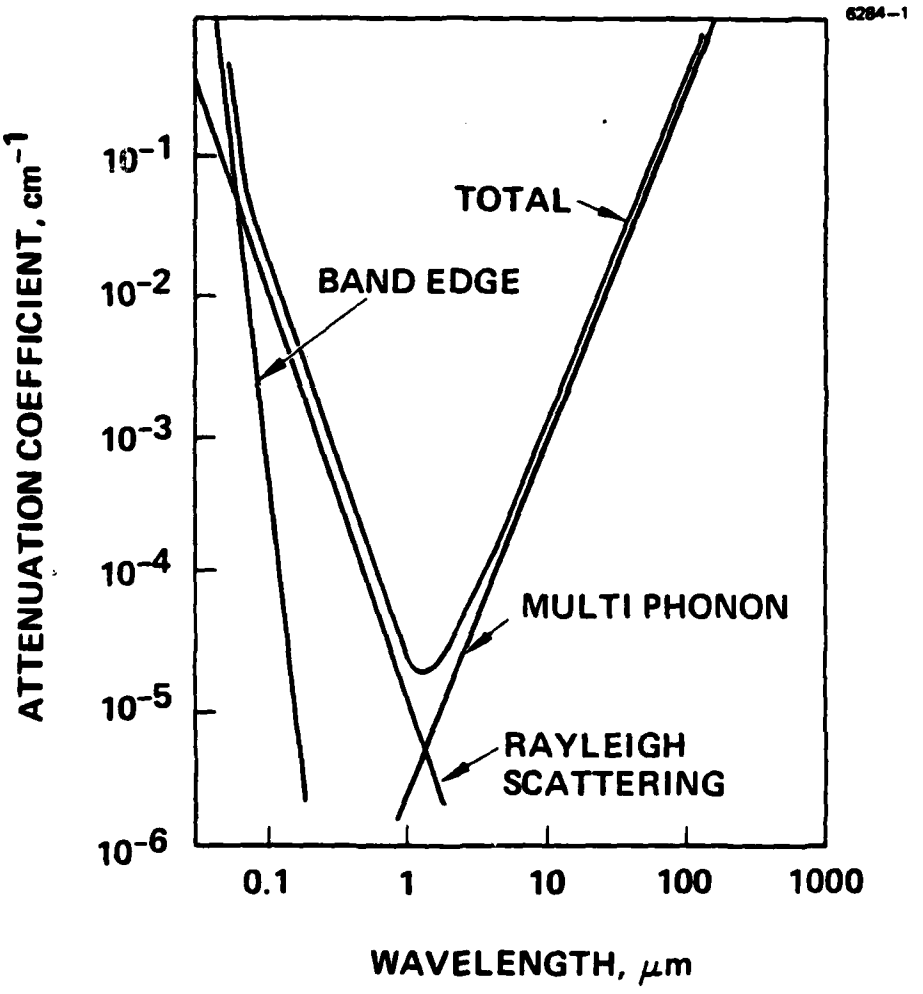
6284-1
ATTENUATION COEFFICIENT, cm^{-1}
10^{-1}
10^{-2}
10^{-3}
10^{-4}
10^{-5}
10^{-6}
TOTAL
BAND EDGE
MULTI PHONON
RAYLEIGH SCATTERING
0.1
1
10
100
1000
WAVELENGTH, μm

Figure 1.

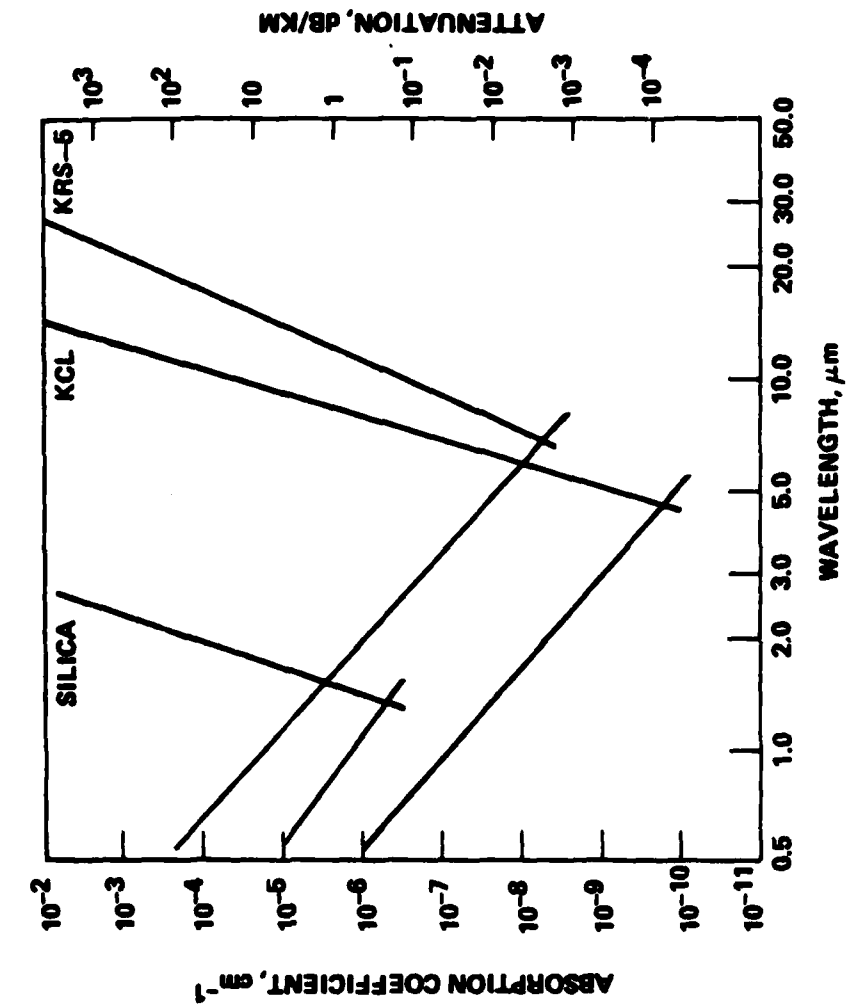
ATTENUATION, dB/KM
10^{-3}
10^{-2}
10
1
10^{-1}
10^{-2}
10^{-3}
10^{-4}
KRS–5
KCL
SILICA
0.5
1.0
2.0
3.0
5.0
10.0
20.0
30.0
50.0
WAVELENGTH, μm
10^{-2}
10^{-3}
10^{-4}
10^{-5}
10^{-6}
10^{-7}
10^{-8}
10^{-9}
10^{-10}
10^{-11}
ABSORPTION COEFFICIENT, cm^{-1}

Figure 2.

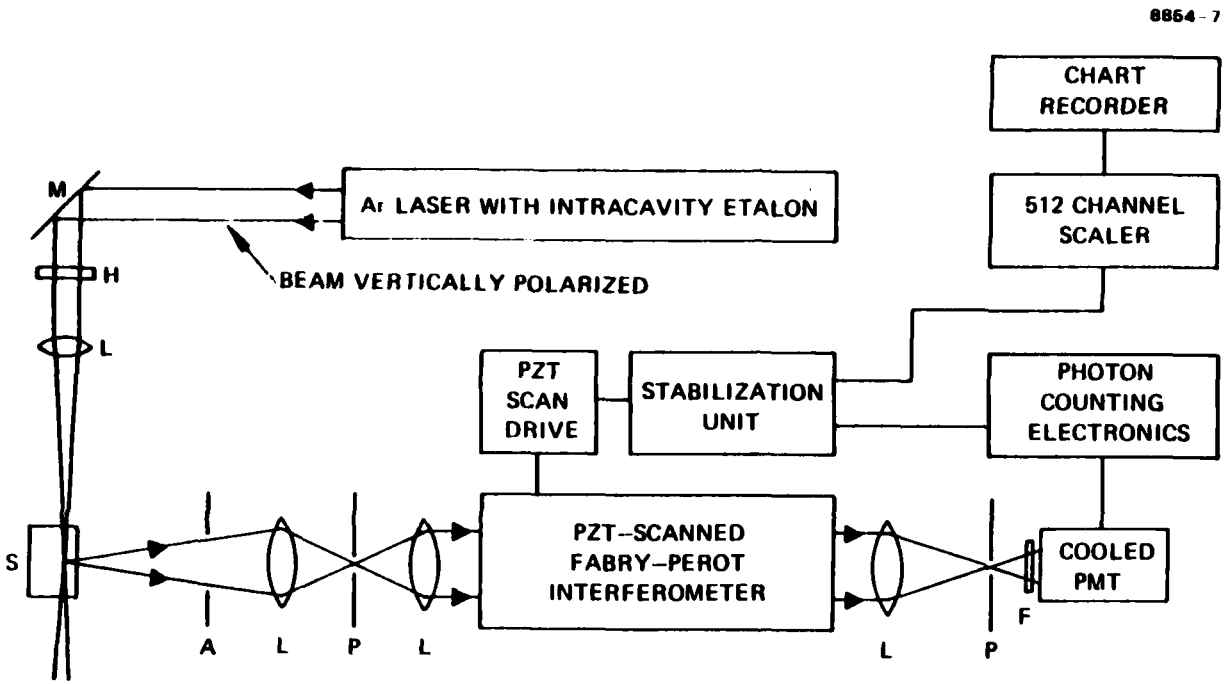

M : PLANE MIRROR
H : HALFWAVE PLATE TO ROTATE POLARIZATION IF DESIRED
L : LENSES TO FOCUS AND COLLIMATE LIGHT
S : TRANSPARENT SAMPLE
A : APERTURE TO LIMIT RANGE OF SCATTERING ANGLES DETECTED
P : PINHOLES TO BLOCK OFF-AXIS LIGHT
F : NARROWBAND (30 Å) FILTER TO BLOCK FLUORESCENCE, RAMAN SCATTERING AND BACKGROUND RADIATION

Figure 3.

Figure 4.

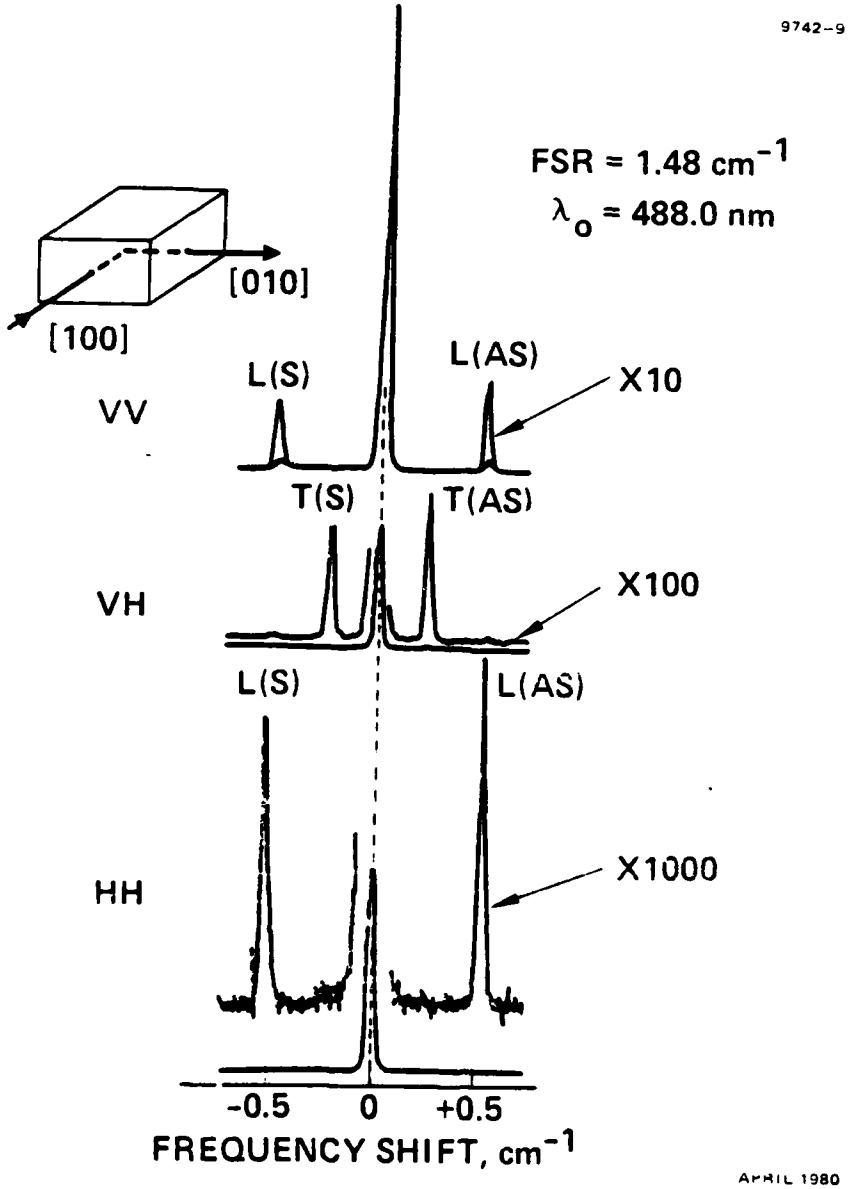
9742-9
FSR = 1.48 cm^{-1}
λ_o = 488.0 nm
[010]
[100]
L(S)
L(AS)
X10
VV
T(S)
T(AS)
VH
X100
L(S)
L(AS)
HH
X1000
-0.5
0
+0.5
FREQUENCY SHIFT, cm^{-1}
APRIL 1980

Figure 5.

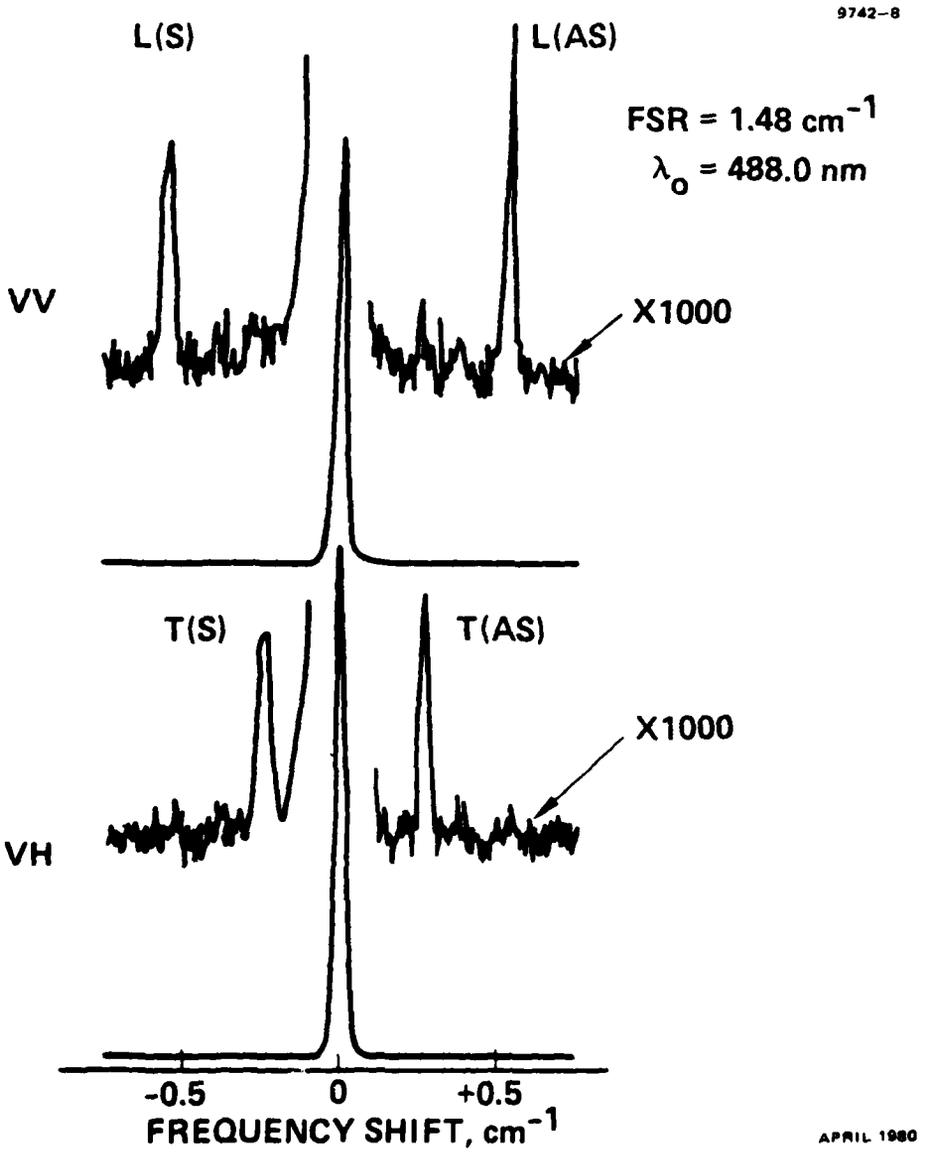
9742-8
L(S)
L(AS)
FSR = 1.48 cm^{-1}
λ_o = 488.0 nm
VV
X1000
T(S)
T(AS)
X1000
VH
-0.5
0
+0.5
FREQUENCY SHIFT, cm^{-1}
APRIL 1980

Figure 6.